5
Multi-Link Manipulator

5.1 INTRODUCTION

The chapter presents the theoretical study to determine the modal parameters and to investigate the dynamic instability of a harmonically driven planar multi-link manipulator with flexible hub and joints which can incorporate an arbitrary number of links and joints. A bidirectional time dependent motion is provided at the actuator representing a Cartesian motion while the flexibilities of joints are modelled as torsional spring-inertia system. The dynamic modeling of representative three-link manipulator has been developed considering the link and joint flexibilities by employing extended Hamilton's principle. The detailed coupled nonlinear equations of motion and corresponding boundary conditions along with governing equations of joint motions are obtained. Further, eigenanalysis with subsequent derivation of mode shapes of the system has been performed to demonstrate the behavior of manipulator under parametric variations. Then, the second-order method of multiple scales has been employed to further analyze the vibration attributes of steady-state responses and their stability under different resonance conditions arising due to the joint motions and inertial coupling. The effect of geometric and inertial coupling existing between the flexible arms on bifurcation states and stability of the obtained solutions has been thoroughly investigated and the results obtained here have been verified and found to be in good agreement. The comparative mode shapes and bifurcation diagrams with varying design parameters that describe the vibrating system have been illustrated to demonstrate the dynamics of the flexible manipulator. Different configurations of the manipulator have been developed by varying the mass and flexibility of the link, payload lifted by link and changing hub-joint parameters. The results obtained provided a useful insight into the vibration characteristics of multi-link flexible manipulator under harmonic hub-joint motions which shall further insure its proper vibration attenuation and control.

5.2 MATHEMATICAL MODELING

A schematic of flexible multi-link manipulator incorporating payload with flexible joints operating in a planar space is shown in Fig. 5.1. The motion of the manipulator is described by a global co-ordinate system represented by (X,Y) with $\left(\hat{X},\hat{Y}\right)$ as the unit vectors are assumed; the moving reference frame of $\left(\hat{x}_i,\hat{y}_i\right)$, $i=1,2,....j$ are the orthogonal unit vectors attached with flexible links. The hub and joints are assumed to undergo planar revolute motions and a bidirectional time dependent motion $\{\vartheta(t),\eta(t)\}$ in Cartesian plane is provided at the actuator. The expressions for the position vector of general point and end-point for jth link are given below:

$$\vec{P}_j=\vec{P}_{(j\text{-}1)L}+\begin{bmatrix}x+u_j\\ w_j+y\end{bmatrix}^{(x_j,y_j)}, \text{ and } \vec{P}_j=\vec{P}_{(j\text{-}1)L}+\begin{bmatrix}L_j+u_{jL}\\ w_{jL}\end{bmatrix}^{(x_j,y_j)}. \tag{5.1}$$

Here, (x,y) denotes the undeformed position of an arbitrary point on the link. The relations between the unit vectors of inertial and moving co-ordinate system for the jth link are given as.

$$\begin{bmatrix}\hat{x}_j\\ \hat{y}_j\end{bmatrix}=\begin{bmatrix}\cos\left(\sum_{k=1}^{j}\dot{\theta}_k+\dot{w}'_{(k-1)L}\right) & \sin\left(\sum_{k=1}^{j}\dot{\theta}_k+\dot{w}'_{(k-1)L}\right)\\ -\sin\left(\sum_{k=1}^{j}\dot{\theta}_k+\dot{w}'_{(k-1)L}\right) & \cos\left(\sum_{k=1}^{j}\dot{\theta}_k+\dot{w}'_{(k-1)L}\right)\end{bmatrix}\begin{bmatrix}\hat{X}\\ \hat{Y}\end{bmatrix}. \tag{5.2}$$

The expressions for the total kinetic energy (T_{total}) and potential energy (U_{total}) of the multi-link manipulator system is expressed in terms of generalized coordinate system, respectively are given by:

$$T_{total}=(1/2)\sum_{i=1}^{j}\left[m_i\dot{P}_{iL}^T\dot{P}_{iL}+\int_0^{L_i}\rho_i\dot{P}_i^T\dot{P}_i+I_{hi}\sum_{k=1}^{i}\left(\dot{\theta}_k+\dot{w}'_{(k-1)L}\right)\right]+(1/2)m_a\left\{\dot{\eta}(t)^2+\dot{\vartheta}(t)^2\right\}. \tag{5.3}$$

$$U_{total}=1/2\left[\sum_{i=1}^{j}\int_0^{L_i}E_iI_i\left(w_i''\right)^2dx+\sum_{i=1}^{j}\int_0^{L_i}E_iA_i\left(u_i'+(1/2)w_i'^2\right)^2dx+\sum_{i=1}^{j}k_i\sum_{k=1}^{i}\left(\dot{\theta}_k+\dot{w}'_{(k-1)L}\right)^2\right]. \tag{5.4}$$

Here, T_{total} comprises kinetic energy associated with masses at the end of links, mass of the links, hub-joint inertias and actuator mass, while U_{total} represents the elastic strain energy of links, energy due to axial stretching and strain energy of flexible joints, respectively.

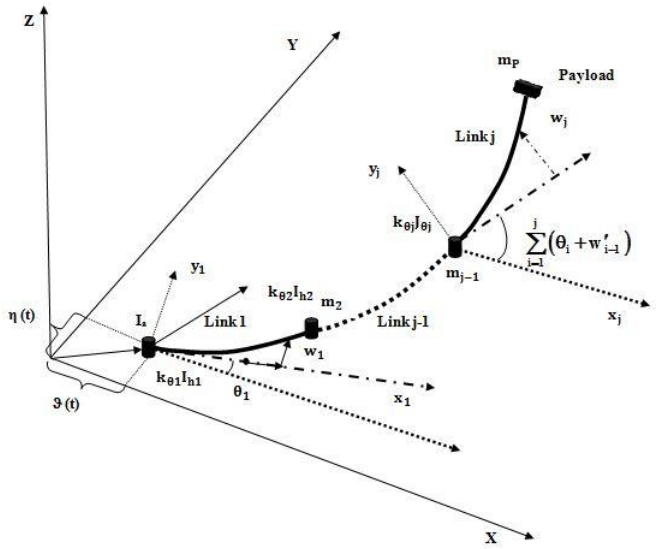

Fig. 5.1: Schematic diagram of multi-link flexible manipulator

5.2.1 Free vibration analysis

Here, to have an understanding of the dynamics of the multi-link manipulator, modeling of a three-link manipulator system driven by prismatic and revolute flexible joints has been presented. The governing equations of motion of links and joints along with the boundary conditions are obtained by substituting Eqs. (5.1)-(5.4) in extended Hamilton's principle.

Equations of motion in longitudinal and transverse direction for first link are expressed as:

$$\{u_1\}:\ \rho_1A_1\left(2\dot{w}_1\dot{\theta}_1+w_1\ddot{\theta}_1-\ddot{u}_1-\ddot{\vartheta}-\theta_1\ddot{\eta}+x\dot{\theta}_1^2+u_1\dot{\theta}_1^2-\theta_1\dot{\vartheta}\dot{\theta}_1\right)+E_1A_1\left(u_1''+w_1'w_2''\right)=0. \tag{5.5}$$

$$\{w_1\}:\ \rho_1A_1\left(w_1\dot{\theta}_1^2+\theta_1\ddot{\vartheta}-2\dot{\theta}_1\dot{u}_1-\theta_1\dot{\theta}_1\dot{\eta}-\dot{w}_1-x\ddot{\theta}_1-u_1\ddot{\theta}_1-\ddot{\eta}\right)+E_1A_1\left\{\left(u_1''+w_1'w_1''\right)w'+\left(u_1'+(1/2)w_1'\right)w_1''\right\}$$
$$-E_1I_1w_1''''=0. \tag{5.6}$$

The associated linearized boundary conditions for the first link are:

$$E_1A_1\left\{u_1'\right\}_{(x=0)}-m_a\left(\ddot{\vartheta}+\ddot{u}_1\right)_{(x=0)}=0,$$

$$\left(\sum_{i=1}^{3}m_i+\sum_{i=2}^{3}\rho_iA_iL_i\right)\left(-\ddot{u}_{1L}-\ddot{\vartheta}\right)-E_1A_1u_{1L}+E_2A_2\left(u_2\right)_{(x=0)}=0. \tag{5.7}$$

$$E_1I_1\left(w_1'''\right)_{(x=0)}-m_a\left(\ddot{\eta}+\ddot{w}_1\right)_{(x=0)}=0,\ E_1I_1w_1'(0,t)=0,$$

$$\int_0^{L_2}\rho_2A_2\left(-x\ddot{w}_2-x\ddot{\eta}-x^2\ddot{w}_{1L}'-x^2\ddot{\theta}_1-x^2\ddot{\theta}_2\right)dx+\left(\sum_{i=2}^{3}m_i+\rho_3A_3\right)\left(-L_2\ddot{w}_{2L}-L_2\ddot{\eta}-{L_2}^2\ddot{w}_{1L}'-{L_2}^2\ddot{\theta}_1-{L_2}^2\ddot{\theta}_2\right)$$

$$+\int_0^{L_3}\rho_3A_3\left\{-x\ddot{w}_3-x^2\ddot{\theta}_1-x^2\ddot{\theta}_2-x^2\ddot{w}_{1L}'-x^2\ddot{w}_{2L}'-x^2\ddot{\theta}_3-x\ddot{\eta}\right\}dx+$$

$$m_3\left(-L_3\ddot{w}_3-{L_3}^2\ddot{\theta}_1-{L_3}^2\ddot{\theta}_2-{L_3}^2\ddot{w}_{1L}'-L_2\ddot{\eta}-{L_3}^2\ddot{w}_{2L}'\right)$$

$$-I_{h2}\left(\ddot{\theta}_1+\ddot{\theta}_2+\ddot{w}_{1L}'\right)-k_{\theta2}\left(\theta_1+\theta_2+w_{1L}'\right)-I_{h3}\left(\ddot{\theta}_1+\ddot{\theta}_2+\ddot{w}_{1L}'+\ddot{w}_{2L}'+\ddot{\theta}_3\right)-k_{\theta3}\left(\theta_1+\theta_2+w_{1L}'+w_{2L}'+\theta_3\right)$$

$$-E_1I_1w_{1L}''+E_2I_2w_2''\left(x=0\right)=0,$$

$$\left(\sum_{i=1}^{3}m_i+\sum_{i=2}^{3}\rho_iA_iL_i\right)\left(-\ddot{w}_{1L}-L_1\ddot{\theta}_1-\ddot{\eta}\right)+E_1I_1w_{1L}'''-E_2I_2w_2'''(0,t)=0. \tag{5.8}$$

Equations of motion in longitudinal and transverse direction for second link are expressed as:

$$\left\{u_2\right\}:\rho_2A_2\begin{pmatrix}-\ddot{u}_2-\ddot{\vartheta}+2\dot{w}_2\dot{\theta}_1+2\dot{w}_2\dot{\theta}_2+2\dot{w}_2\dot{w}_{1L}'+w_2\ddot{\theta}_1+w_2\ddot{\theta}_2+\\ w_2\ddot{w}_{1L}'-\theta_1\ddot{\eta}-\theta_2\ddot{\eta}-w_{1L}'\ddot{\eta}+u_2\dot{\theta}_1^{\,2}+u_2\dot{\theta}_2^{\,2}+u_2\dot{w}_{1L}'^{\,2}+\\ 2u_2\dot{\theta}_1\dot{\theta}_2+2u_2\dot{\theta}_1\dot{w}_{1L}'+2u_2\dot{\theta}_2\dot{w}_{1L}'+x\dot{\theta}_1^{\,2}+x\dot{\theta}_2^{\,2}+x\dot{w}_{1L}'^{\,2}\\ +2x\dot{\theta}_1\dot{\theta}_2+2x\dot{\theta}_1\dot{w}_{1L}'+2x\dot{\theta}_2\dot{w}_{1L}'-\theta_1\dot{\vartheta}\dot{\theta}_1-\theta_2\dot{\vartheta}\dot{\theta}_2-w_{1L}'\dot{\vartheta}\dot{w}_{1L}'-\\ \theta_2\dot{\vartheta}\dot{\theta}_1-w_{1L}'\dot{\vartheta}\dot{\theta}_1-\theta_1\dot{\vartheta}\dot{\theta}_2-w_{1L}'\dot{\vartheta}\dot{\theta}_2-\theta_1\dot{\vartheta}\dot{w}_{1L}'-\theta_2\dot{\vartheta}\dot{w}_{1L}'\end{pmatrix}+E_2A_2\left(u_2'+w_2'w_2''\right)=0. \tag{5.9}$$

$$\left\{w_2\right\}:\ \rho_2A_2\begin{pmatrix}-2u_2\dot{\theta}_1-2u_2\dot{\theta}_2-2u_2\dot{w}_{1L}'+w_2\dot{\theta}_1^{\,2}+w_2\dot{\theta}_2^{\,2}+w_2\dot{w}_{1L}'^{\,2}+2w_2\dot{\theta}_1\dot{\theta}_2+2w_2\dot{\theta}_2\dot{w}_{1L}'\\ +2w_2\dot{w}_{1L}'\dot{\theta}_1-\theta_1\dot{\eta}\dot{\theta}_1-\theta_2\dot{\eta}\dot{\theta}_1-w_{1L}'\dot{\eta}\dot{\theta}_1-\theta_1\dot{\eta}\dot{\theta}_2-\theta_2\dot{\eta}\dot{\theta}_2-w_{1L}'\dot{\eta}\dot{\theta}_2-\theta_1\dot{\eta}\dot{w}_{1L}'\\ -\theta_2\dot{\eta}\dot{w}_{1L}'-w_{1L}'\dot{\eta}\dot{w}_{1L}'-\dot{w}_2-\dot{\eta}-u_2\ddot{\theta}_1-u_2\ddot{\theta}_2-u_2\ddot{w}_{1L}'-x\ddot{\theta}_1-x\ddot{\theta}_2-x\ddot{w}_{1L}'+\\ \theta_1\ddot{\vartheta}+\theta_2\ddot{\vartheta}+w_{1L}'\ddot{\vartheta}\end{pmatrix} \tag{5.10}$$

$$-E_2I_2w''''+E_2A_2\left\{\left(u_2'+w_2'w_2''\right)w_2'+\left(u_2'+w_2'/2\right)w_2''\right\}=0.$$

The associated linearized boundary conditions for the second link are:

$$E_2A_2u_{2(0,t)}=E_1A_1u_{1L},\ \left(\sum_{i=2}^{3}m_i+\rho_3A_3L_3\right)\left(-\ddot{u}_{3L}-\ddot{\vartheta}\right)-E_2A_2u_{2L}+E_3A_3\left\{u_3\right\}_{(x=0)}=0. \tag{5.11}$$

$$E_2I_2w_2\left(0,t\right)=E_1I_1w_{1L},\ E_2I_2w_2'\left(0,t\right)=E_1I_1w_{1L}',$$

$$\int_0^{L_3}\rho_3A_3\left\{-x\ddot{w}_3-x^2\ddot{\theta}_1-x^2\ddot{\theta}_2-x^2\ddot{w}_{1L}'-x^2\ddot{w}_{2L}'-x^2\ddot{\theta}_3-x\ddot{\eta}\right\}dx+m_3\begin{Bmatrix}-L_3\ddot{w}_3-{L_3}^2\ddot{\theta}_1-{L_3}^2\ddot{\theta}_2-{L_3}^2\ddot{w}_{1L}'-\\ {L_3}^2\ddot{w}_{2L}'-{L_3}^2\ddot{\theta}_3-L_3\ddot{\eta}\end{Bmatrix}-$$

$$I_{h3}\left(\ddot{\theta}_1+\ddot{\theta}_2+\ddot{w}_{1L}'+\ddot{w}_{2L}'+\ddot{\theta}_3\right)-k_{\theta3}\left(\theta_1+\theta_2+w_{1L}'+w_{2L}'+\theta_3\right)-E_2I_2w_{2L}''+\left(E_3I_3w_3''\right)_{(x=0)}=0,$$

$$\left(\sum_{i=2}^{3}m_i+\rho_3A_3L_3\right)\left(-\ddot{w}_{2L}-\ddot{\eta}-L_2\ddot{\theta}_1-L_2\ddot{\theta}_2-L_2\ddot{w}_{1L}'\right)+E_2I_2w_{2L}'''-\left(E_3I_3w_3'''\right)_{(x=0)}=0. \tag{5.12}$$

Equations of motion in longitudinal and transverse direction for third link are expressed as:

$$\{u_3\}: \rho_3 A_3 \begin{pmatrix} -\ddot{u}_3 - \ddot{\vartheta} + 2\dot{w}_3\dot{\theta}_1 + 2\dot{w}_3\dot{\theta}_2 + 2\dot{w}_3\dot{w}'_{1L} + 2\dot{w}_3\dot{w}'_{2L} + 2\dot{w}_3\dot{\theta}_3 + w_3\ddot{\theta}_1 + w_3\ddot{\theta}_2 + w_3\ddot{w}'_{1L} + \\ w_3\ddot{w}'_{2L} + w_3\ddot{\theta}_3 - \theta_1\ddot{\eta} - \theta_2\ddot{\eta} - w'_{1L}\ddot{\eta} - w'_{2L}\ddot{\eta} - \theta_3\ddot{\eta} + x\dot{\theta}_1^{\,2} + x\dot{\theta}_2^{\,2} + x\dot{w}'^{\,2}_{1L} + x\dot{w}'^{\,2}_{2L} + \\ x\dot{\theta}_3^{\,2} + u_3\dot{\theta}_1^{\,2} + u_3\dot{\theta}_2^{\,2} + u_3\dot{w}'^{\,2}_{1L} + u_3\dot{w}'^{\,2}_{2L} + u_3\dot{\theta}_3^{\,2} + 2x\dot{\theta}_1\dot{\theta}_2 + 2x\dot{\theta}_1\dot{w}'_{1L} + 2x\dot{\theta}_1\dot{w}'_{2L} \\ +2x\dot{\theta}_1\dot{\theta}_3 + 2x\dot{\theta}_2\dot{w}'_{1L} + 2x\dot{\theta}_2\dot{w}'_{2L} + 2x\dot{\theta}_2\dot{\theta}_3 + 2x\dot{w}'_{1L}\dot{w}'_{2L} + 2x\dot{w}'_{1L}\dot{\theta}_3 + 2x\dot{w}'_{2L}\dot{\theta}_3 + \\ 2u_3\dot{\theta}_1\dot{\theta}_2 + 2u_3\dot{\theta}_1\dot{w}'_{1L} + 2u_3\dot{\theta}_1\dot{w}'_{2L} + 2u_3\dot{\theta}_1\dot{\theta}_3 + 2u_3\dot{\theta}_2\dot{w}'_{1L} + 2u_3\dot{\theta}_2\dot{w}'_{2L} + 2u_3\dot{\theta}_2\dot{\theta}_3 + \\ 2u_3\dot{w}'_{1L}\dot{w}'_{2L} + 2u_3\dot{w}'_{1L}\dot{\theta}_3 + 2u_3\dot{w}'_{2L}\dot{\theta}_3 - \theta_1\dot{\vartheta}\dot{\theta}_1 - \theta_1\dot{\vartheta}\dot{\theta}_2 - \theta_1\dot{\vartheta}\dot{w}'_{1L} - \theta_1\nu\dot{\vartheta}\dot{w}'_{2L} - \theta_1\dot{\vartheta}\dot{\theta}_3 \\ -\theta_2\dot{\vartheta}\dot{\theta}_1 - \theta_2\dot{\vartheta}\dot{\theta}_2 - \theta_2\dot{\vartheta}\dot{w}'_{1L} - \theta_2\dot{\vartheta}\dot{w}'_{2L} - \theta_2\dot{\vartheta}\dot{\theta}_3 - w'_{1L}\dot{\vartheta}\dot{\theta}_1 - w'_{1L}\dot{\vartheta}\dot{\theta}_2 - w'_{1L}\dot{\vartheta}\dot{w}'_{1L} - \\ w'_{1L}\dot{\vartheta}\dot{w}'_{2L} - w'_{1L}\dot{\vartheta}\dot{\theta}_3 - w'_{2L}\dot{\vartheta}\dot{\theta}_1 - w'_{2L}\dot{\vartheta}\dot{\theta}_2 - w'_{2L}\dot{\vartheta}\dot{w}'_{1L} - w'_{2L}\dot{\vartheta}\dot{w}'_{2L} - w'_{2L}\dot{\vartheta}\dot{\theta}_3 - \\ \theta_3\dot{\vartheta}\dot{\theta}_1 - \theta_3\dot{\vartheta}\dot{\theta}_2 - \theta_3\dot{\vartheta}\dot{w}'_{1L} - \theta_3\dot{\vartheta}\dot{w}'_{2L} - \theta_3\dot{\vartheta}\dot{\theta}_3 \end{pmatrix} \tag{5.13}$$

$$+E_3A_3\left(u_3'' + w_3'w_3''\right) = 0.$$

$$\{w_3\}: \rho_3 A_3 \begin{pmatrix} -2u_3\dot{\theta}_1 - 2u_3\dot{\theta}_2 - 2u_3\dot{w}'_{1L} - 2u_3\dot{w}'_{2L} - 2u_3\dot{\theta}_3 + w_3\dot{\theta}_1^{\,2} + w_3\dot{\theta}_2^{\,2} + w_3\dot{w}'^{\,2}_{1L} + w_3\dot{w}'^{\,2}_{2L} + \\ w_3\dot{\theta}_3^{\,2} + 2w_3\dot{\theta}_1\dot{\theta}_2 + 2w_3\dot{w}'_{1L}\dot{\theta}_1 + 2w_3\dot{\theta}_1\dot{\theta}_3 + 2w_3\dot{w}'_{2L}\dot{\theta}_1 + 2w_3\dot{\theta}_2\dot{\theta}_3 + 2w_3\dot{w}'_{1L}\dot{\theta}_1 + \\ 2w_3\dot{w}'_{2L}\dot{\theta}_2 + 2w_3\dot{w}'_{1L}\dot{\theta}_3 + 2w_3\dot{w}'_{1L}\dot{w}'_{2L} + 2w_3\dot{w}'_{2L}\dot{\theta}_3 - \theta_1\dot{\eta}\dot{\theta}_1 - \theta_2\dot{\eta}\dot{\theta}_1 - w'_{1L}\dot{\eta}\dot{\theta}_1 - \\ w'_{2L}\dot{\eta}\dot{\theta}_1 - \theta_3\dot{\eta}\dot{\theta}_1 - \theta_1\dot{\eta}\dot{\theta}_2 - \theta_2\dot{\eta}\dot{\theta}_2 - w'_{1L}\dot{\eta}\dot{\theta}_2 - w'_{2L}\dot{\eta}\dot{\theta}_2 - \theta_3\dot{\eta}\dot{\theta}_2 - \theta_1\dot{\eta}\dot{w}'_{1L} - \theta_2\dot{\eta}\dot{w}'_{1L} - \\ w'_{1L}\dot{\eta}\dot{w}'_{1L} - w'_{2L}\dot{\eta}\dot{w}'_{1L} - \theta_3\dot{\eta}\dot{w}'_{1L} - \theta_1\dot{\eta}\dot{w}'_{2L} - \theta_2\dot{\eta}\dot{w}'_{2L} - w'_{1L}\dot{\eta}\dot{w}'_{2L} - w'_{2L}\dot{\eta}\dot{w}'_{2L} - \\ \theta_3\dot{\eta}\dot{w}'_{2L} - \theta_1\dot{\eta}\dot{\theta}_3 - \theta_2\dot{\eta}\dot{\theta}_3 - w'_{1L}\dot{\eta}\dot{\theta}_3 - w'_{2L}\dot{\eta}\dot{\theta}_3 - \theta_3\dot{\eta}\dot{\theta}_3 - \ddot{w}_3 - \ddot{\eta} - x\ddot{\theta}_1 - x\ddot{\theta}_2 - \\ x\ddot{w}'_{1L} - x\ddot{w}'_{2L} - x\ddot{\theta}_3 - u_3\ddot{\theta}_1 - u_3\ddot{\theta}_2 - u_3\ddot{w}'_{1L} - u_3\ddot{w}'_{2L} - u_3\ddot{\theta}_3 + \theta_1\ddot{\vartheta} + \theta_2\ddot{\vartheta} + w'_{1L}\ddot{\vartheta} + \\ w'_{2L}\ddot{\vartheta} + \theta_3\ddot{\vartheta} \end{pmatrix} \tag{5.14}$$

$$-E_3I_3w_3'''' + E_3A_3\left\{\left(u_3'' + w_3'w_3''\right)w_3' + \left(u_3' + (1/2)w_3'\right)w_3''\right\} = 0.$$

The associated linearized boundary conditions for the third link are:

$$E_3A_3u_{3(0,t)} = E_2A_2u_{2L},\ \ m_3\left(-\ddot{u}_{3L} - \ddot{\vartheta}\right) - E_3A_3u_{3L} = 0. \tag{5.15}$$

$$\left(E_3I_3w_3\right)_{(0,t)} = E_3I_3w_{3L},\ \left(E_3I_3w_3'\right)_{(0,t)} = E_2I_2w'_{2L},\ E_3I_3w''_{3L} = 0,$$

$$m_3\left(-\ddot{w}_{3L} - \ddot{\eta} - L_3\ddot{\theta}_1 - L_3\ddot{\theta}_2 - L_3\ddot{w}'_{1L} - L_3\ddot{w}'_{2L} - L_3\ddot{\theta}_3\right) - E_3I_3w'''_{3L} = 0. \tag{5.16}$$

The linearized governing equation of first joint motion is expressed as:

$$\begin{aligned} &\int_0^{L_1}\rho_1A_1\left(-x\ddot{w}_1 - x^2\ddot{\theta}_1 - x\ddot{\eta}\right)dx + \left(\sum_{i=1}^{3}m_i + \sum_{i=2}^{3}\rho_iA_iL_i\right)\left(-L_1\ddot{w}_{1L} - L_1^{\,2}\ddot{\theta}_1 - L_1\ddot{\eta}\right) \\ &+\int_0^{L_2}\rho_2A_2\left(-x\ddot{w}_2 - x\ddot{\eta} - x^2\ddot{w}'_{1L} - x^2\ddot{\theta}_1 - x^2\ddot{\theta}_2\right)dx + \left(\sum_{i=2}^{3}m_i + \rho_3A_3L_3\right)\begin{pmatrix} -L_2\ddot{w}_{2L} - L_2\ddot{\eta} - L_2^{\,2}\ddot{w}'_{1L} - \\ L_2^{\,2}\ddot{\theta}_1 - L_2^{\,2}\ddot{\theta}_2 \end{pmatrix} \\ \{\theta_1\}: &+\int_0^{L_2}\rho_3A_3\left\{-x\ddot{w}_3 - x^2\ddot{\theta}_1 - x^2\ddot{\theta}_2 - x^2\ddot{w}'_{1L} - x^2\ddot{w}'_{2L} - x^2\ddot{\theta}_3\right\}dx + m_3\begin{Bmatrix} -L_3\ddot{w}_3 - L_3^{\,2}\ddot{\theta}_1 - L_3^{\,2}\ddot{\theta}_2 - L_3^{\,2}\ddot{w}'_{1L} - L_3^{\,2}\ddot{w}'_{2L} - \\ L_3^{\,2}\ddot{\theta}_3 - L_3\ddot{\eta} \end{Bmatrix} \\ &-J_a\ddot{\theta}_a - k_{\theta a}\theta_a - J_1\left(\ddot{\theta}_1 + \ddot{\theta}_2 + \ddot{w}'_{1L}\right) - k_{\theta 1}\left(\theta_1 + \theta_2 + w'_{1L}\right) - J_2\left(\ddot{\theta}_1 + \ddot{\theta}_2 + \ddot{w}'_{1L} + \ddot{w}'_{2L} + \ddot{\theta}_3\right) - \\ &k_{\theta 1}\left(\theta_1 + \theta_2 + w'_{1L} + w'_{2L} + \theta_3\right) = 0. \end{aligned} \tag{5.17}$$

The linearized governing equation of second joint motion is expressed as:

$$\begin{aligned} &\int_0^{L_2}\rho_2A_2\left(-x\ddot{w}_2 - x\ddot{\eta} - x^2\ddot{w}'_{1L} - x^2\ddot{\theta}_1 - x^2\ddot{\theta}_2\right)dx + \left(\sum_{i=2}^{3}m_i + \rho_3A_3L_3\right)\left(-L_2\ddot{w}_{2L} - L_2\ddot{\eta} - L_2^{\,2}\ddot{w}'_{1L} - L_2^{\,2}\ddot{\theta}_1 - L_2^{\,2}\ddot{\theta}_2\right) \\ \{\theta_3\}: &+\int_0^{L_2}\rho_3A_3\left\{-x\ddot{w}_3 - x^2\ddot{\theta}_1 - x^2\ddot{\theta}_2 - x^2\ddot{w}'_{1L} - x^2\ddot{w}'_{2L} - x^2\ddot{\theta}_3 - x\ddot{\eta}\right\}dx + m_3\begin{Bmatrix} -L_3\ddot{w}_3 - L_3^{\,2}\ddot{\theta}_1 - L_3^{\,2}\ddot{\theta}_2 - L_3^{\,2}\ddot{w}'_{1L} - \\ L_3^{\,2}\ddot{w}'_{2L} - L_3^{\,2}\ddot{\theta}_3 - L_3\ddot{\eta} \end{Bmatrix} \\ &-J_1\left(\ddot{\theta}_1 + \ddot{\theta}_2 + \ddot{w}'_{1L}\right) - k_{\theta 1}\left(\theta_1 + \theta_2 + w'_{1L}\right) - J_2\left(\ddot{\theta}_1 + \ddot{\theta}_2 + \ddot{w}'_{1L} + \ddot{w}'_{2L} + \ddot{\theta}_3\right) - k_{\theta 1}\left(\theta_1 + \theta_2 + w'_{1L} + w'_{2L} + \theta_3\right) = 0. \end{aligned} \tag{5.18}$$

The linearized governing equation of third joint motion is expressed as:

$$\{\theta_3\}: \int_0^{L_2} \rho_3 A_3 \left\{-x\ddot{w}_3 - x^2\ddot{\theta}_1 - x^2\ddot{\theta}_2 - x^2\ddot{w}'_{1L} - x^2\ddot{w}'_{2L} - x^2\ddot{\theta}_3 - x\ddot{\eta}\right\} dx + m_3 \begin{Bmatrix} -L_3\ddot{w}_3 - L_3{}^2\ddot{\theta}_1 - L_3{}^2\ddot{\theta}_2 - L_3{}^2\ddot{w}'_{1L} - \\ L_3{}^2\ddot{w}'_{2L} - L_3{}^2\ddot{\theta}_3 - L_3\ddot{\eta} \end{Bmatrix} \qquad (5.19)$$

$$-J_2\left(\ddot{\theta}_1 + \ddot{\theta}_2 + \ddot{w}'_{1L} + \ddot{w}'_{2L} + \ddot{\theta}_3\right) - k_{\theta 1}\left(\theta_1 + \theta_2 + w'_{1L} + w'_{2L} + \theta_3\right) = 0.$$

For modal analysis of a 3R manipulator, the coupled nonlinear, Cartesian motion at hub and axial terms from Eqs. (5.5)-(5.19) are neglected and further expressing the transverse deflections of the links in terms of new functions in space and time as: $s_1(x,t) = w_1(x,t) + x\theta_1$, $s_2(x,t) = w_2(x,t) + x\left(\theta_1 + \theta_2 + w'_{1L}\right)$ and $s_3(x,t) = w_3(x,t) + x\left(\theta_1 + \theta_2 + \theta_3 + w'_{1L} + w'_{2L}\right)$. The procedure followed in section 4.3.1 is adopted here to obtain the mode shapes of the links as:

$$W_1^n(\bar{x}) = P_1{}^n \cos\left(\bar{\delta}^n \bar{x}\right) + P_2{}^n \sin\left(\bar{\delta}^n \bar{x}\right) + P_3{}^n \cosh\left(\bar{\delta}^n \bar{x}\right) + P_4{}^n \sinh\left(\bar{\delta}^n \bar{x}\right),$$

$$W_2^n(\bar{x}) = Q_1{}^n \cos\left(\mu_1 \bar{\delta}^n \bar{x}\right) + Q_2{}^n \sin\left(\mu_1 \bar{\delta}^n \bar{x}\right) + Q_3{}^n \cosh\left(\mu_1 \bar{\delta}^n \bar{x}\right) + Q_4{}^n \sinh\left(\mu_1 \bar{\delta}^n \bar{x}\right),$$

$$W_3^n(\bar{x}) = R_1{}^n \cos\left(\mu_2 \bar{\delta}^n \bar{x}\right) + R_2{}^n \sin\left(\mu_2 \bar{\delta}^n \bar{x}\right) + R_3{}^n \cosh\left(\mu_2 \bar{\delta}^n \bar{x}\right) + R_4{}^n \sinh\left(\mu_2 \bar{\delta}^n \bar{x}\right). \qquad (5.20)$$

A set of twelve algebraic equations with $\left(P_1 \cdots P_4, Q_1 \cdots Q_4, R_1 \cdots R_4\right)^n$ as variables in terms of known system parameters and characteristics exponent $\left(\bar{\delta}^n\right)$ is obtained by substituting Eq. **Error! Reference source not found.** into the boundary conditions and the elements of the coefficient matrix are given below:

$$K_{11} = \left(\cos\left(\bar{\delta}^n\right) + \bar{\delta}^n \sin\left(\bar{\delta}^n\right) - 1\right) \Big/ \left(\bar{\delta}^n\right)^2 + \left(\alpha_{M1}\alpha_{L1} + \alpha_{M2}\alpha_{L2} + \alpha_{m1} + \alpha_{m2} + \alpha_{m3}\right)\cos\left(\bar{\delta}^n\right)$$

$$K_{12} = \left(\sin\left(\bar{\delta}^n\right) - \bar{\delta}^n \cos\left(\bar{\delta}^n\right)\right) \Big/ \left(\bar{\delta}^n\right)^2 + \left(\alpha_{M1}\alpha_{L1} + \alpha_{M2}\alpha_{L2} + \alpha_{m1} + \alpha_{m2} + \alpha_{m3}\right)\sin\left(\bar{\gamma}_m\right) +$$

$$\bar{\delta}^n \alpha_{Ih1}\left(1 - \Omega_{h1}{}^2\right)$$

$$K_{13} = \left(\bar{\delta}^n \sinh\left(\bar{\delta}^n\right) - \cosh\left(\bar{\delta}^n\right) + 1\right) \Big/ \left(\bar{\delta}^n\right)^2 + \left(\alpha_{M1}\alpha_{L1} + \alpha_{M2}\alpha_{L2} + \alpha_{m1} + \alpha_{m2} + \alpha_{m3}\right)\cosh\left(\bar{\delta}^n\right)$$

$$K_{14} = \left(\bar{\delta}^n \cosh\left(\bar{\delta}^n\right) - \sinh\left(\bar{\delta}^n\right)\right) \Big/ \left(\bar{\delta}^n\right)^2 + \left(\alpha_{M1}\alpha_{L1} + \alpha_{M2}\alpha_{L2} + \alpha_{m1} + \alpha_{m2} + \alpha_{m3}\right)\sinh\left(\bar{\delta}^n\right) +$$

$$\bar{\delta}^n \alpha_{Ih1}\left(1 - \Omega_{h1}{}^2\right)$$

$$K_{21}, K_{23} = 1,\ K_{31} = \left(\alpha_{M1}\alpha_{L1} + \alpha_{M2}\alpha_{L2} + \alpha_{m1} + \alpha_{m2} + \alpha_{m3}\right)\bar{\delta}^n \cos\left(\bar{\delta}^n\right) + \sin\left(\bar{\delta}^n\right),$$

$$K_{32} = \left(\alpha_{M1}\alpha_{L1} + \alpha_{M2}\alpha_{L2} + \alpha_{m1} + \alpha_{m2} + \alpha_{m3}\right)\bar{\delta}^n \sin\left(\bar{\delta}^n\right) - \cos\left(\bar{\delta}^n\right),$$

$$K_{33} = \left(\alpha_{M1}\alpha_{L1} + \alpha_{M2}\alpha_{L2} + \alpha_{m1} + \alpha_{m2} + \alpha_{m3}\right)\bar{\delta}^n \cosh\left(\bar{\delta}^n\right) + \sinh\left(\bar{\delta}^n\right),$$

$$K_{34}^n = \left(\alpha_{M1}\alpha_{L1} + \alpha_{M2}\alpha_{L2} + \alpha_{m1} + \alpha_{m2} + \alpha_{m3}\right)\bar{\delta}^n \sinh\left(\bar{\delta}^n\right) + \cosh\left(\bar{\delta}^n\right),\ K_{36} = \chi_1 \mu_1{}^3,\ K_{38} = \chi_1 \mu_1{}^3,$$

$$K_{41}^n = -\cos\left(\bar{\delta}^n\right),\ K_{42}^n = -\sin\left(\bar{\delta}^n\right),\ K_{43}^n = \cosh\left(\bar{\delta}^n\right),\ K_{44}^n = \sinh\left(\bar{\delta}^n\right),\ K_{45} = \chi_1 \mu_1{}^2,\ K_{47}^n = -\chi_1 \mu_1{}^2,$$

$$K_{51}^n = -\alpha_{Ih2}\left(1 - \Omega_{h2}^2\right)\bar{\delta}^n \sin\left(\bar{\delta}^n\right),\ K_{52} = \alpha_{Ih2}\left(1 - \Omega_{h2}^2\right)\bar{\delta}^n \left\{\cos\left(\bar{\delta}^n\right) - 1\right\},$$

$$K_{53} = \alpha_{Ih2}\left(1 - \Omega_{h2}^2\right)\bar{\delta}^n \sinh\left(\bar{\delta}^n\right),\ K_{54} = \alpha_{Ih2}\left(1 - \Omega_{h2}^2\right)\bar{\delta}^n \left\{\sinh\left(\bar{\delta}^n\right) - 1\right\},$$

$$K_{55} = -\chi_1 \begin{bmatrix} \left\{\alpha_{M1} \Big/ \left(\mu_1 \bar{\delta}^n\right)^2\right\}\left\{\cos\left(\lambda_1 \bar{\delta}^n\right) + \lambda_1 \bar{\delta}^n \sin\left(\lambda_1 \bar{\delta}^n\right) - 1\right\} + \\ \left(\alpha_{M2}\alpha_{L2} + \alpha_{m2} + \alpha_{m3}\right)\alpha_{L1} \cos\left(\lambda_1 \bar{\delta}^n\right) \end{bmatrix},$$

$$K_{56} = -\chi_1 \begin{bmatrix} \left\{\alpha_{M1} \Big/ \left(\mu_1 \bar{\delta}^n\right)^2\right\}\left\{\sin\left(\lambda_1 \bar{\delta}^n\right) - \lambda_1 \bar{\delta}^n \cos\left(\lambda_1 \bar{\delta}^n\right)\right\} + \left(\alpha_{M2}\alpha_{L2} + \alpha_{m2} + \alpha_{m3}\right)\alpha_{L1} \sin\left(\lambda_1 \bar{\delta}^n\right) \\ + \mu_1 \bar{\delta}^n \alpha_{Ih2}\left(1 - \Omega_{h2}^2\right) \end{bmatrix},$$

$$K_{57} = -\chi_1\left[\left\{\alpha_{M1}\Big/\left(\mu_1\bar{\delta}^n\right)^2\right\}\left\{\lambda_1\bar{\delta}^n\sinh\left(\lambda_1\bar{\delta}^n\right)-\cosh\left(\lambda_1\bar{\delta}^n\right)+1\right\}+\left(\alpha_{M2}\alpha_{L2}+\alpha_{m2}+\alpha_{m3}\right)\alpha_{L1}\cosh\left(\lambda_1\bar{\delta}^n\right)\right],$$

$$K_{58} = -\chi_1\left[\begin{array}{l}\left\{\alpha_{M1}\Big/\left(\mu_1\bar{\delta}^n\right)^2\right\}\left\{\lambda_1\bar{\delta}^n\cosh\left(\lambda_1\bar{\delta}^n\right)-\sinh\left(\lambda_1\bar{\delta}^n\right)\right\}+\left(\alpha_{M2}\alpha_{L2}+\alpha_{m2}+\alpha_{m3}\right)\alpha_{L1}\sinh\left(\lambda_1\bar{\delta}^n\right)\\ +\mu_1\bar{\gamma}_m\alpha_{Ih2}\left(1-\Omega_{h2}^2\right)\end{array}\right],$$

$K_{61} = \cos\left(\bar{\delta}^n\right)$, $K_{62} = \sin\left(\bar{\delta}^n\right)-\bar{\delta}^n$, $K_{63} = \cosh\left(\bar{\delta}^n\right)$, $K_{64} = \sinh\left(\bar{\delta}^n\right)-\bar{\delta}^n$, $K_{65} = -\chi_1$, $K_{67} = -\chi_1$,

$K_{75} = -\chi_1\mu_1^2\cos\left(\lambda_1\bar{\delta}^n\right)$, $K_{76} = -\chi_1\mu_1^2\sin\left(\lambda_1\bar{\delta}^n\right)$, $K_{77} = \chi_1\mu_1^2\cosh\left(\lambda_1\bar{\delta}^n\right)$, $K_{77} = \chi_1\mu_1^2\sinh\left(\lambda_1\bar{\delta}^n\right)$,

$K_{79} = \chi_2\mu_2^2$, $K_{711} = -\chi_2\mu_2^2$, $K_{85} = \left(\alpha_{M2}\alpha_{L2}+\alpha_{m2}+\alpha_{m3}\right)\bar{\delta}^n\cos\left(\lambda_1\bar{\delta}^n\right)+\chi_1\mu_1^3\sin\left(\lambda_1\bar{\delta}^n\right)$,

$K_{86} = \left(\alpha_{M2}\alpha_{L2}+\alpha_{m2}+\alpha_{m3}\right)\bar{\delta}^n\sin\left(\lambda_1\bar{\delta}^n\right)-\chi_1\mu_1^3\cos\left(\lambda_1\bar{\delta}^n\right)$,

$K_{87} = \left(\alpha_{M2}\alpha_{L2}+\alpha_{m2}+\alpha_{m3}\right)\bar{\delta}^n\cosh\left(\lambda_1\bar{\delta}^n\right)+\chi_1\mu_1^3\sinh\left(\lambda_1\bar{\delta}^n\right)$, $K_{810} = \chi_2\mu_2^3$, $K_{812} = -\chi_2\mu_2^3$,

$K_{91} = -\bar{\delta}^n\alpha_{Ih3}\left(1-\Omega_{h3}^2\right)\sin\left(\bar{\delta}^n\right)$, $K_{92} = \bar{\delta}^n\alpha_{Ih3}\left(1-\Omega_{h3}^2\right)\left\{\cos\left(\bar{\delta}^n\right)-1\right\}$,

$K_{93} = \bar{\delta}^n\alpha_{Ih3}\left(1-\Omega_{h3}^2\right)\sinh\left(\bar{\delta}^n\right)$, $K_{94} = \bar{\delta}^n\alpha_{Ih3}\left(1-\Omega_{h3}^2\right)\left\{\cosh\left(\bar{\delta}^n\right)-1\right\}$,

$K_{95} = -\bar{\delta}^n\chi_1\mu_1\alpha_{Ih3}\left(1-\Omega_{h3}^2\right)\sin\left(\lambda_1\bar{\delta}^n\right)$, $K_{96} = \bar{\delta}^n\chi_1\mu_1\alpha_{Ih3}\left(1-\Omega_{h3}^2\right)\left\{\cos\left(\lambda_1\bar{\delta}^n\right)-1\right\}$,

$K_{97} = \bar{\delta}^n\chi_1\mu_1\alpha_{h3}\left(1-\Omega_{h3}^2\right)\sinh\left(\lambda_1\bar{\delta}^n\right)$, $K_{98} = \bar{\delta}^n\chi_1\mu_1\alpha_{Ih3}\left(1-\Omega_{h3}^2\right)\left\{\cosh\left(\lambda_1\bar{\delta}^n\right)-1\right\}$,

$$K_{99} = -\chi_2\left[\left\{\alpha_{M2}\Big/\left(\mu_2\bar{\delta}^n\right)^2\right\}\left\{\cos\left(\lambda_2\bar{\delta}^n\right)+\lambda_2\bar{\delta}^n\sin\left(\lambda_2\bar{\delta}^n\right)-1\right\}+\alpha_{m3}\alpha_{L2}\cos\left(\lambda_2\bar{\delta}^n\right)\right],$$

$$K_{910} = -\chi_2\left[\left\{\alpha_{M2}\Big/\left(\mu_2\bar{\delta}^n\right)^2\right\}\left\{\sin\left(\lambda_2\bar{\delta}^n\right)-\lambda_2\bar{\delta}^n\cos\left(\lambda_2\bar{\delta}^n\right)\right\}+\alpha_{m3}\alpha_{L2}\sin\left(\lambda_2\bar{\delta}^n\right)+\mu_2\bar{\delta}^n\alpha_{Ih3}\left(1-\Omega_{h3}^2\right)\right],$$

$$K_{911} = -\chi_2\left[\left\{\alpha_{M2}\Big/\left(\mu_2\bar{\delta}^n\right)^2\right\}\left\{\lambda_2\bar{\delta}^n\sinh\left(\lambda_2\bar{\delta}^n\right)-\cosh\left(\lambda_2\bar{\delta}^n\right)+1\right\}+\alpha_{m3}\alpha_{L2}\cosh\left(\lambda_2\bar{\delta}^n\right)\right],$$

$$K_{912} = -\chi_2\left[\left\{\alpha_{M2}\Big/\left(\mu_2\bar{\delta}^n\right)^2\right\}\left\{\lambda_2\bar{\delta}^n\cosh\left(\lambda_2\bar{\delta}^n\right)-\sinh\left(\lambda_2\bar{\delta}^n\right)\right\}+\alpha_{m3}\alpha_{L2}\sinh\left(\lambda_2\bar{\delta}^n\right)+\mu_2\bar{\delta}^n\alpha_{Ih3}\left(1-\Omega_{h3}^2\right)\right],$$

$K_{101} = -\bar{\delta}^n\sin\left(\bar{\delta}^n\right)$, $K_{102} = \bar{\delta}^n\left\{\sin\left(\bar{\delta}^n\right)-1\right\}$, $K_{103} = \bar{\delta}^n\sinh\left(\bar{\delta}^n\right)$, $K_{104} = \bar{\delta}^n\left(\cosh\left(\bar{\delta}^n\right)-1\right)$,

$K_{105} = \chi_1 c\left(\lambda_1\bar{\delta}^n\right)$, $K_{106} = \chi_1\left\{\sin\left(\lambda_1\bar{\delta}^n\right)-\lambda_1\bar{\delta}^n\right\}$, $K_{107} = \chi_1\cosh\left(\lambda_1\bar{\delta}^n\right)$,

$K_{108} = \chi_1\left\{\sinh\left(\lambda_1\bar{\delta}^n\right)-\lambda_1\bar{\delta}^n\right\}$, $K_{109} = -\chi_2$, $K_{1011} = -\chi_2$,

$K_{1109} = \alpha_{m3}\bar{\delta}^n\cos\left(\lambda_2\bar{\delta}^n\right)+\chi_2\mu_2^2\sin\left(\lambda_2\bar{\delta}^n\right)$, $K_{1110} = \alpha_{m3}\bar{\delta}^n\sin\left(\lambda_2\bar{\delta}^n\right)-\chi_2\mu_2^2\cos\left(\lambda_2\bar{\delta}^n\right)$,

$K_{1111} = \alpha_{m3}\bar{\delta}^n\cosh\left(\lambda_2\bar{\delta}^n\right)+\chi_2\mu_2^2\sinh\left(\lambda_2\bar{\delta}^n\right)$, $K_{1112} = \alpha_{m3}\bar{\delta}^n\sinh\left(\lambda_2\bar{\delta}^n\right)+\chi_2\mu_2^2\cosh\left(\lambda_2\bar{\delta}^n\right)$,

$K_{1209} = -\cos\left(\lambda_2\bar{\delta}^n\right)$, $K_{1210} = -\sin\left(\lambda_2\bar{\delta}^n\right)$, $K_{1211} = \cosh\left(\lambda_2\bar{\delta}^n\right)$, $K_{1112} = \sinh\left(\lambda_2\bar{\delta}^n\right)$,

$K_{15}, K_{16}, K_{17}, K_{18}, K_{19}, K_{110}, K_{111}, K_{112}, K_{22}, K_{24}, K_{25}, K_{26}, K_{27}, K_{28}, K_{29}, K_{210}, K_{211}, K_{212}, K_{35}$,
$K_{37}, K_{39}, K_{310}, K_{311}, K_{312}, K_{46}, K_{48}, K_{49}, K_{410}, K_{411}, K_{412}, K_{59}, K_{510}, K_{511}, K_{512}, K_{66}, K_{68}, K_{69}$,
$K_{610}, K_{611}, K_{612}, K_{71}, K_{72}, K_{73}, K_{74}, K_{710}, K_{712}, K_{81}, K_{82}, K_{83}, K_{84}, K_{89}, K_{811}, K_{1010}, K_{1012}, K_{1101}$,
$K_{1102}, K_{1103}, K_{1104}, K_{1105}, K_{1106}, K_{1107}, K_{1108}, K_{1201}, K_{1202}, K_{1203}, K_{1204}, K_{1205}, K_{1206}, K_{1207}, K_{1208} = 0$, (5.21)

The nondimensional parameters appearing in above equations are:

$\delta^4 = \rho_1 A_1\omega_m^2 / E_1 I_1$, $\chi_1 = E_2 I_2 / E_1 I_1$, $\chi_2 = E_3 I_3 / E_1 I_1$, $\alpha_{M1} = \rho_2 A_2 / \rho_1 A_1$,
$\alpha_{M2} = \rho_3 A_3 / \rho_1 A_1$, $\mu_1{}^4 = \alpha_{M1} / \chi_1$, $\mu_2{}^4 = \alpha_{M2} / \chi_2$, $\bar{\delta} = \delta L_1$, $\alpha_{L1} = L_2 / L_1$, $\alpha_{L2} = L_3 / L_1$,
$\alpha_{m1} = m_1 / \rho_1 A_1 L_1$, $\alpha_{m2} = m_2 / \rho_1 A_1 L_1$, $\alpha_{m3} = m_3 / \rho_1 A_1 L_1$, $\alpha_{Ih1} = I_{h1} / \rho_1 A_1 L_1{}^3$,

$\alpha_{Ih2} = I_{h2} / \rho_1 A_1 L_1^3$,

$\alpha_{Ih3} = I_{h3} / \rho_1 A_1 L_1^3$, $\Omega_{h1} = \left((k_{\theta 1} / I_{h1}) / \omega_m^2 \right)$, $\Omega_{h2} = \left((k_{\theta 2} / I_{h2}) / \omega_m^2 \right)$, $\Omega_{h3} = \left((k_{\theta 3} / I_{h3}) / \omega_m^2 \right)$,

$\lambda_1 = \mu_1 \alpha_{L1}$, and $\lambda_2 = \mu_2 \alpha_{L2}$, (5.22)

The condition for the existence of non-trivial solution for the set of equations obtained earlier, i.e. $\left| K\left(\bar{\delta}^n\right) \right| = 0$, results in the eigenfrequency equation of the system in terms of nondimensional parameters defined in Eq. (5.22); here $K\left(\bar{\delta}^n\right)$ denotes the coefficient matrix. In order to obtain the mode shapes of the links obtained in Eq. (5.20), the constants $\left(P_2 - P_4, Q_1 - Q_4, R_1 - R_4\right)^n$ are expressed in terms of unit magnitude P_1^n.

5.2.2 Dynamic Characterization

Now, the governing flexible equations of motion of the links and rigid body motion of the joints given in Eqs. (5.6), (5.10), (5.14), (5.17), (5.18) & (5.19) are arranged in a computationally efficient closed form of equations using assumed mode method. The obtained set of equations is numerically simulated by input smooth sinusoidal torque and the parametric variation of the system responses is studied. An expression similar to Eq. (4.114) using the mode shapes obtained in Eq. (5.20) are used to obtain the dynamic model of the 3R manipulator in state space form as:

$$\left[M\left(q_{1,2,3}\right) \right] \begin{bmatrix} q_{1tt} \\ q_{2tt} \\ q_{3tt} \\ \theta_{1tt} \\ \theta_{2tt} \\ \theta_{3tt} \end{bmatrix} + \eta\left(q_{1,2,3t}, \theta_{1,2,3t}\right) \begin{bmatrix} q_{1t} \\ q_{2t} \\ q_{3t} \\ \theta_{1t} \\ \theta_{2t} \\ \theta_{3t} \end{bmatrix} + \begin{bmatrix} \zeta_1\left(q_{1t}, \theta_{1t}\right) \\ \zeta_1\left(q_{1,2t}, \theta_{1,2t}\right) \\ \zeta_1\left(q_{1,2,3t}, \theta_{1,2,3t}\right) \\ 0 \\ 0 \\ 0 \end{bmatrix} = \begin{bmatrix} 0 \\ 0 \\ 0 \\ \tau_1 \\ \tau_2 \\ \tau_3 \end{bmatrix} \tag{5.23}$$

Here, $M\left(q_{1,2,3}\right)$, $\eta\left(q_{1,2,3t}, \theta_{1,2,3t}\right)$, and $\left[\zeta\left(q_{1,2,3}, \theta_{1,2,3t}\right) \right]$ respectively are the mass matrix, coriolis component matrix and stiffness matrix and $\left[\tau_{1,2,3} \right]$ represent the input torques at the joint of the links.

5.2.3 Nonlinear forced vibration analysis

The frequency response of the multi-link manipulator is investigated for the existence of forced and 1:1:1 internal resonance in the manipulator links due to the inertial coupling between the links. A small amplitude excitation is provided to the first link and the influence of system parameters on the nonlinear characteristics of other links is studied. The hub- joint dynamics and axial deformation in governing equations of motion of links obtained in Eqs. (5.6), (5.10), and (5.14) are neglected; geometric nonlinearities components are retained and structural damping in the links have been included. With a similar approach as in section 4.5.4, the nondimensionalized and appropriately ordered governing equations of motion of the links are obtained as:

$$\ddot{p}_1(\tau) + \Omega_1{}^2 p_1(\tau) + \left\{ 2\xi_1 \dot{p}_1 - \beta_1 \cos\left(\omega_1 \tau\right) - \beta_2 p_1 \sin^2\left(\omega_1 \tau\right) - \beta_3 p_1{}^3(\tau) \right\} = 0. \tag{5.24}$$

$$\ddot{p}_2(\tau) + \Omega_2{}^2 p_2(\tau) + \varepsilon \begin{Bmatrix} 2\xi_2 \dot{p}_2 - \beta_4 \cos\left(\omega_1 \tau\right) - \beta_5 \cos\left(\omega_2 \tau\right) + \beta_6 \ddot{p}_1 - \beta_7 p_2 \sin^2\left(\omega_1 \tau\right) - \\ \beta_8 p_2 \sin^2\left(\omega_2 \tau\right) - \beta_9 p_2 \dot{p}_1{}^2 - \beta_{10} p_2 \sin\left(\omega_1 \tau\right) \sin\left(\omega_2 \tau\right) + \\ \beta_{11} p_2 \dot{p}_1 \sin\left(\omega_1 \tau\right) + \beta_{12} p_2 \dot{p}_1 \sin\left(\omega_2 \tau\right) - \beta_{13} p_2{}^3(\tau) \end{Bmatrix} = 0. \tag{5.25}$$

$$\ddot{p}_3(\tau)+\Omega_3{}^2 p_3(\tau)++\varepsilon\begin{Bmatrix}2\xi_3\dot{p}_3-\beta_{14}\cos(\omega_1\tau)-\beta_{15}\cos(\omega_2\tau)+\beta_{16}\ddot{p}_1-\beta_{17}\cos(\omega_3\tau)-\\ \beta_{19}p_3\sin^2(\omega_1\tau)-\beta_{20}p_3\sin^2(\omega_2\tau)-\beta_{21}p_3\dot{p}_1{}^2-\beta_{22}p_3\sin^2(\omega_3\tau)-\\ \beta_{23}p_3\dot{p}_2{}^2-\beta_{24}p_3\sin(\omega_1\tau)\sin(\omega_2\tau)+\beta_{25}p_3\dot{p}_1\sin(\omega_1\tau)+\beta_{18}\ddot{p}_2-\\ \beta_{26}p_3\sin(\omega_1\tau)\sin(\omega_3\tau)+\beta_{27}p_3\dot{p}_2\sin(\omega_1\tau)+\beta_{28}p_3\dot{p}_1\sin(\omega_2\tau)-\\ \beta_{29}p_3\sin(\omega_2\tau)\sin(\omega_3\tau)+\beta_{30}p_3\dot{p}_2\sin(\omega_2\tau)+\beta_{31}p_3\dot{p}_1\sin(\omega_3\tau)-\\ \beta_{32}p_3\dot{p}_1\dot{p}_2+\beta_{33}p_3\dot{p}_2\sin(\omega_3\tau)-\beta_{34}p_3{}^3(\tau)\end{Bmatrix}=0. \quad (5.26)$$

The nonlinear equations of motions obtained in Eqs. (5.24)-(5.26) can be solved by various numerical methods. To simplify the complex differential problem in hand cannot be routinely solved, one can take the advantage of the small parameter ε, and hence, the most commonly used perturbation method, method of multiple scales is exploited. Here, the deflections p_i are expressed in terms of fast (T_0) and slow time (T_1) scales to obtain the steady-state solutions of Eqs. (5.24)-(5.26) as:

$$p_i=p_{i0}(T_0,T_1)+p_{i1}(T_0,T_1),\ i=1,2,3. \quad (5.27)$$

Error! No sequence specified. Error! No sequence specified. Error! No sequence specified. Using chain rule for the time derivatives, substituting Eqs. (5.27) in Eqs. (5.24)-(5.26) and after equating the coefficients of the same powers of ε, following equations for first, second and third link are obtained as:

First link:

$$O(\varepsilon^0):\ \partial^2 p_{10}/\partial T_0{}^2+\Omega_1{}^2 p_{10}=0. \quad (5.28)$$

$$O(\varepsilon^1):\ \begin{aligned}&\partial^2 p_{11}/\partial T_1{}^2+\Omega_1{}^2 p_{11}+2\xi_1(\partial p_{10}/\partial T_0)+2\left(\partial^2 p_{10}/\partial T_0\partial T_1\right)-\beta_1\cos(\omega_1 T_0)-\\ &\beta_2 p_{10}\sin^2(\omega_1 T_0)-\beta_3 p_{10}{}^3=0.\end{aligned} \quad (5.29)$$

Second link:

$$O(\varepsilon^0):\ \partial^2 p_{20}/\partial T_0{}^2+\Omega_2{}^2 p_{20}=0. \quad (5.30)$$

$$O(\varepsilon^1):\ \begin{aligned}&\partial^2 p_{21}/\partial T_1{}^2+\Omega_2{}^2 p_{21}+2\xi_2(\partial p_{20}/\partial T_0)+2\left(\partial^2 p_{20}/\partial T_0\partial T_1\right)-\beta_4\cos(\omega_1 T_0)-\\ &\beta_5\cos(\omega_2 T_0)+\beta_6\left(\partial^2 p_{10}/\partial T_0^2\right)-\beta_7 p_{20}\sin^2(\omega_1 T_0)-\beta_8 p_{20}\sin^2(\omega_2 T_0)-\\ &\beta_9 p_{20}(\partial p_{10}/\partial T_0)^2-\beta_{13}p_{20}{}^3-\beta_{10}p_{20}\sin(\omega_1 T_0)\sin(\omega_2 T_0)+\\ &\beta_{11}p_{20}(\partial p_{10}/\partial T_0)\sin(\omega_1 T_0)+\beta_{12}p_{20}(\partial p_{10}/\partial T_0)\sin(\omega_2 T_0)=0.\end{aligned} \quad (5.31)$$

Third link:

$$O(\varepsilon^0):\ \partial^2 p_{30}/\partial T_0{}^2+\Omega_3{}^2 p_{30}=0. \quad (5.32)$$

$$O(\varepsilon^1):\ \begin{aligned}&\partial^2 p_{31}/\partial T_1{}^2+\Omega_3{}^2 p_{31}+2\xi_3(\partial p_{30}/\partial T_0)+2\left(\partial^2 p_{30}/\partial T_0\partial T_1\right)-\beta_{14}\cos(\omega_1 T_0)-\\ &\beta_{15}\cos(\omega_2 T_0)+\beta_{16}\left(\partial^2 p_{10}/\partial T_0^2\right)-\beta_{17}\cos(\omega_3 T_0)+\beta_{18}\left(\partial^2 p_{20}/\partial T_0^2\right)-\\ &\beta_{19}p_{30}\sin^2(\omega_1 T_0)-\beta_{20}p_{30}\sin^2(\omega_2 T_0)-\beta_{21}p_{30}(\partial p_{10}/\partial T_0)^2-\\ &\beta_{22}p_{30}\sin^2(\omega_3 T_0)-\beta_{23}p_{30}(\partial p_{20}/\partial T_0)^2-\beta_{24}p_{30}\sin(\omega_1 T_0)\sin(\omega_2 T_0)\\ &+\beta_{25}p_{30}(\partial p_{10}/\partial T_0)\sin(\omega_1 T_0)-\beta_{26}p_{30}\sin(\omega_1 T_0)\sin(\omega_3 T_0)+\\ &\beta_{27}p_{30}(\partial p_{20}/\partial T_0)\sin(\omega_1 T_0)+\beta_{28}p_{30}(\partial p_{10}/\partial T_0)\sin(\omega_2 T_0)-\\ &\beta_{29}p_{30}\sin(\omega_2 T_0)\sin(\omega_3 T_0)+\beta_{30}p_{30}(\partial p_{20}/\partial T_0)\sin(\omega_2 T_0)+\\ &\beta_{31}p_{30}(\partial p_{10}/\partial T_0)\sin(\omega_3 T_0)-\beta_{32}p_{30}(\partial p_{10}/\partial T_0)(\partial p_{20}/\partial T_0)+\\ &\beta_{30}p_{30}(\partial p_{20}/\partial T_0)\sin(\omega_3 T_0)-\beta_{34}p_{30}{}^3=0.\end{aligned} \quad (5.33)$$

The general solutions of ordinary differential equations Eqs. (5.28), (5.30) & (5.32) are:

$$p_{10} = G(T_0)e^{i\Omega_1 T_0} + \bar{G}(T_1)e^{i\Omega_1 T_0}. \tag{5.34}$$

$$p_{20} = H(T_0)e^{i\Omega_2 T_0} + \bar{H}(T_1)e^{i\Omega_2 T_0}. \tag{5.35}$$

$$p_{30} = I(T_0)e^{i\Omega_3 T_0} + \bar{I}(T_1)e^{i\Omega_3 T_0}. \tag{5.36}$$

Now, substituting Eqs. (5.34)-(5.36) simultaneously in Eqs. (5.29), (5.31) & (5.33), the resultant equations are obtained containing secular or small divisor terms at different resonance conditions which result in unbounded solutions. From the resulting equations, the system experience different resonance conditions such as primary resonance case $\omega_1 \approx \Omega_1$, $\omega_2 \approx \Omega_2$, $\omega_3 \approx \Omega_3$; internal resonance case $\Omega_1 \approx \Omega_2$, $\Omega_2 \approx \Omega_3$, $\Omega_3 \approx \Omega_1$; combined resonance case $\omega_1 + \omega_2 \approx 2\Omega_2$, $\omega_1 + \omega_2 \approx 2\Omega_3$, $\omega_1 + \omega_3 \approx 2\Omega_3$, $\omega_3 + \omega_2 \approx 2\Omega_3$, and simultaneous resonances occurring with the combination of above resonance conditions.

5.2.4 1:1:1 Internal Resonance $\left(\Omega_1 \approx \Omega_2 \approx \Omega_3\right)$

It is found numerically that the internal resonance of 1:1:1 exist between the links of the manipulator system, i.e., Ω_1, Ω_2, and Ω_3 are nearly equal to each other for certain system parameters. This internal resonance can be avoided by changing the length of the links and hence varying $\left(\alpha_{L1,2}\right)$. In the present case, nonlinear free vibration case has been analyzed by giving a small initial excitation to the first link and investigating the influence of system parameters on the vibration behavior of the second and third links due to the existence of internal resonance. The harmonic motions given to the joints are neglected from Eqs. (5.24)-(5.26). Further, the nearness of Ω_1 to Ω_2 for internal resonance condition in the first two links are expressed as $\Omega_2 + \varepsilon\sigma_1$, and Ω_2 to Ω_3 for internal resonance condition in last two links are, respectively expressed as $\Omega_3 + \varepsilon\sigma_2$, here $\left(\sigma_{1,2}\right)$ are known as detuning parameters. Now, using the procedure explained in subsection 3.2.3 and eliminating the secular terms leading to unbounded solutions, the following expressions are obtained:

$$2i\Omega_1\left(\partial G/\partial T_1\right) + 2i\Omega_1\xi_1 G - 3\beta_3 G^2\bar{G} = 0. \tag{5.37}$$

$$\begin{aligned}&2i\Omega_2\left(\partial H/\partial T_1\right) - 2\Omega_2\mu_2 H - \beta_6{\Omega_1}^2 G\exp\left(i\sigma_1 T_1\right) - 3\beta_{13}H^2\bar{H} + \\ &\beta_9{\Omega_1}^2\left\{G^2\bar{H}\exp\left(2i\sigma_1 T_1\right) - 2G\bar{G}H\right\} = 0.\end{aligned} \tag{5.38}$$

$$\begin{aligned}&2i\Omega_3\left(\partial I/\partial T_1\right) - 2i\Omega_3\xi_3 I - \beta_{16}{\Omega_1}^2 G\exp\left\{i\left(\sigma_1+\sigma_2\right)T_1\right\} - \beta_{18}{\Omega_2}^2 H\exp\left(i\sigma_2 T_1\right) \\ &+\beta_{21}{\Omega_1}^2\left[G^2\bar{I}\exp\left\{i\left(2\sigma_1+2\sigma_1\right)T_1\right\} - 2G\bar{G}I\right] + \beta_{23}{\Omega_2}^2\left\{H^2\bar{I}\exp\left(2i\sigma_1 T_1\right) - 2H\bar{H}I\right\} \\ &+\beta_{32}\Omega_1\Omega_2\left[G\bar{H}I\exp\left\{i\left(\sigma_1+2\sigma_1\right)T_1\right\} - G\bar{H}I\exp\left(i\sigma_1 T_1\right) - \bar{G}HI\exp\left(-i\sigma_1 T_1\right)\right] - 3\beta_{34}I^2\bar{I} = 0.\end{aligned} \tag{5.39}$$

Now, the polar form of $G(T_1)$, $H(T_1)$, $I(T_1)$ expressed respectively as $G(T_1)=(1/2)a_1(T_1)\mathrm{e}^{\mathrm{i}\phi_1(T_1)}$, $H(T_1)=(1/2)a_2(T_1)\mathrm{e}^{\mathrm{i}\phi_2(T_1)}$, and $I(T_1)=(1/2)a_3(T_1)\mathrm{e}^{\mathrm{i}\phi_3(T_1)}$ and substituted in Eqs. (5.37)-(5.39) to obtain the governing equations for the modulation amplitude and phases of respective links.

$$-\Omega_1\left(\partial a_1/\partial T_1\right) - \Omega_1\xi_1 a_1 = 0,\ a_1\Omega_1\left(\partial\phi_1/\partial T_1\right) + (3/8)\beta_3 a_1^3 = 0. \tag{5.40}$$

$$\begin{aligned}&\Omega_2\left(\partial a_2/\partial T_1\right) + \Omega_2\xi_2 a_2 - \left(\beta_6\Omega_1^2 a_1/2\right)\sin\left(\varphi_1\right) + \left(\beta_9\Omega_1^2 a_1^2 a_2/8\right)\sin\left(2\varphi_1\right) = 0, \\ &a_2\Omega_2\left(\partial\varphi_1/\partial T_1\right) - \Omega_2 a_2\sigma_1 + \left(\beta_9\Omega_2 a_1^2 a_2/8\Omega_1\right) - \left(\beta_6{\Omega_1}^2 a_1/2\right)\cos\left(\varphi_1\right) + \left(\beta_9\Omega_1^2 a_1^2 a_2/8\right)\cos\left(2\varphi_1\right) \\ &-\left(\beta_9{\Omega_1}^2 a_1^2 a_2/4\right) - \left(3\beta_{13}a_2^3/8\right) = 0, \varphi_1 = \sigma_1 T_1 - \phi_2 + \phi_1.\end{aligned} \tag{5.41}$$

$$\Omega_3\left(\partial a_3/\partial T_1\right)+\Omega_3\mu_3 a_3-\left(\beta_{16}\Omega_1^2 a_1/2\right)\sin\left(\varphi_1+\varphi_2\right)+\left(\beta_{21}\Omega_1^2 a_1^2 a_3/8\right)\sin\left(2\varphi_1+2\varphi_2\right)$$
$$-\left(\beta_{18}\Omega_2^2 a_2/2\right)\sin\left(\varphi_2\right)+\left(\beta_{23}\Omega_2^2 a_2^2 a_3/8\right)\sin\left(2\varphi_2\right)+$$
$$\left(\beta_{23}\Omega_1\Omega_2 a_1 a_2 a_3/8\right)\left\{\sin\left(\varphi_1+2\varphi_2\right)-\sin\left(\varphi_1\right)-\sin\left(-\varphi_1\right)\right\}=0,$$
$$a_3\Omega_3\left(\partial\varphi_1/\partial T_1+\partial\varphi_2/\partial T_1\right)-\Omega_3 a_3\left(\sigma_1+\sigma_2\right)+\left(3\beta_{21}\Omega_3 a_1^2 a_3/8\Omega_1\right)-\left(\beta_{16}\Omega_1^2 a_1/2\right)\cos\left(\varphi_1+\varphi_2\right)$$
$$-\left(\beta_{18}\Omega_2^2 a_2/2\right)\cos\left(\varphi_2\right)+\left(\beta_{21}\Omega_1^2 a_1^2 a_3/8\right)\cos\left(2\varphi_1+2\varphi_2\right)+\left(\beta_{23}\Omega_2^2 a_2^2 a_3/8\right)\cos\left(2\varphi_2\right)+$$
$$\left(\beta_{32}\Omega_1\Omega_2 a_1 a_2 a_3/8\right)\left\{\cos\left(\varphi_1+2\varphi_2\right)-\cos\left(\varphi_1\right)-\cos\left(-\varphi_1\right)\right\}-\left(\beta_{21}\Omega_1^2 a_1^2 a_3/4\right)-\quad (5.42)$$
$$\left(\beta_{23}\Omega_2^2 a_2^2 a_3/4\right)-\left(3\beta_{34}a_3^3/8\right)=0,\varphi_2=\sigma_2 T_1+\phi_2-\phi_3.$$

The first order approximate solutions of links in terms of original time variable τ, are expressed as:

$$p_1=0.5a_1\cos\left(\Omega_1\tau-\varphi_1\right)+\mathrm{O}\left(\varepsilon\right),\ p_2=0.5a_2\cos\left(\Omega_1\tau+\phi_1-\varphi_1\right)+\mathrm{O}\left(\varepsilon\right),$$
$$p_3=0.5a_3\cos\left(\Omega_1\tau+\phi_1-\varphi_1-\varphi_2\right)+\mathrm{O}\left(\varepsilon\right). \quad (5.43)$$

The steady-state response of the second and third link can be obtained by eliminating the terms involving temporal changes in modulation amplitudes and phases in Eqs. (5.40)-(5.42) i.e. $\partial a_2/\partial T_1,\partial a_3/\partial T_1,\partial\varphi_1/\partial T_1,\partial\varphi_2/\partial T_1=0.$ The elimination of phases i.e. φ_1,φ_2, from the resultant equations results in the sixth-order polynomial in terms of amplitudes $\left(a_1,a_2,a_3\right)$ and detuning parameters $\left(\sigma_1,\sigma_2\right)$. The stability of the steady-state solutions for the second link is ascertained by introducing a small perturbation $\left(a_{21},\lambda_{11}\right)$ in a_2,λ_1 as $a_2=a_{20}+a_{21}$, $\varphi_1=\varphi_{10}+\varphi_{11}$ and investigating the eigenvalues of the following resultant Jacobian matrix:

$$\begin{Bmatrix}\dot{a}_2\\ \dot{\varphi}_1\end{Bmatrix}=\begin{bmatrix}-\xi_2-\left(\beta_9\Omega_1^2 a_{10}^2/8\Omega_2\right)\sin\left(2\varphi_{10}\right) & -\left(\beta_6\Omega_1^2 a_{10}/2\Omega_2\right)\cos\left(\varphi_{10}\right)-\left(\beta_9\Omega_1^2 a_{10}^2 a_{20}/4\Omega_2\right)\cos\left(2\varphi_{10}\right)\\ \sigma_1/\Omega_2 a_{20}+9\beta_{13}a_{20}^2/8\Omega_2-3\beta_3 a_{10}^2\Omega_1/8\Omega_2-\left(\beta_9\Omega_1^2 a_{10}^2/8a_{20}\Omega_2\right)\cos\left(2\varphi_{10}\right)+\beta_9\Omega_1^2 a_{10}^2/4a_{20}\Omega_2 & -\left(\beta_6\Omega_1^2 a_{10}/2\,a_{20}\Omega_2\right)\sin\left(\varphi_{10}\right)+\left(\beta_9\Omega_1^2 a_{10}^2/4\Omega_2\right)\sin\left(2\varphi_{10}\right)\end{bmatrix}\begin{Bmatrix}a_{10}\\ \varphi_{10}\end{Bmatrix}.$$

If the eigenvalues of coefficient matrix $[J]$ have negative real parts the solution is stable, otherwise unstable. The stability of the steady-state solutions of Eq. **Error! Reference source not found.**can also be determined in a similar manner.

5.2.5 Primary Resonance in the links $\left(\omega_1\approx\Omega_1\right),\left(\omega_2\approx\Omega_2\right),\left(\omega_3\approx\Omega_3\right)$

The primary resonance occurs in all the links of the manipulator when the frequency of the driving harmonic joint motion becomes equal or nearly equal to the normalized frequency of the link. Here the internal resonance has been avoided by considering different lengths of the links by changing $\alpha_{L1,2}$. For the primary resonance case, the nearness of ω_i to Ω_i can be expressed as $\omega_i=\Omega_i+\varepsilon\sigma_i$. Now, substituting these expressions along with the Eqs. (5.34)-(5.36) in Eqs. (5.29), (5.31) & (5.33) and eliminating the secular terms for the bounded solutions, following equations are obtained:

$$\Omega_1\left(\partial b_1/\partial T_1\right)-\xi_1\Omega_1 b_1-\beta_1\sin\left(\pi_1\right)/2+\beta_2 b_1\sin\left(2\pi_1\right)/8=0,\pi_1=\sigma_3 T_1-\phi_3,$$
$$b_1\Omega_1\left(\partial\pi_1/\partial T_1\right)-\Omega_1 b_1\sigma_3-\beta_1\cos\left(\pi_1\right)/2-\beta_2 b_1/2+\beta_2 b_1\cos\left(2\pi_1\right)/8-3\beta_3 b_1^3/8=0. \quad (5.44)$$
$$\Omega_2\left(\partial b_2/\partial T_1\right)-\xi_2\Omega_2 b_2-\beta_5\sin\left(\pi_2\right)/2+\beta_8 b_2\sin\left(2\pi_2\right)/8=0,\pi_2=\sigma_4 T_1-\phi_4,$$
$$b_2\Omega_2\left(\partial\pi_2/\partial T_1\right)-\Omega_2 b_2\sigma_4-\beta_5\cos\left(\pi_2\right)/2-\left(b_2/2\right)\left(\beta_8+\beta_7+\beta_9\Omega_1^2 b_1^2/2\right)+$$
$$\beta_8 b_2\cos\left(2\pi_2\right)/8-3\beta_{13}b_2^3/8=0. \quad (5.45)$$

$$\Omega_3\left(\partial b_3/\partial T_1\right)-\xi_3\Omega_3 b_3-\beta_{17}\sin\left(\pi_3\right)/2+\beta_{22}b_3\sin\left(2\pi_3\right)/8=0,\pi_3=\sigma_5 T_1-\phi_5,$$
$$b_3\Omega_3\left(\partial\pi_3/\partial T_1\right)-\Omega_3 b_3\sigma_5-\beta_{17}\cos\left(\pi_3\right)/2-\left(b_2/2\right)\left(\beta_{19}+\beta_{20}+\beta_{21}\Omega_1^2 b_1^2/2+\beta_{23}\Omega_2^2 b_2^2/2\right)+$$
$$\beta_{22}b_3\cos\left(2\pi_3\right)/8-3\beta_{34}b_3^3/8=0. \tag{5.46}$$

The frequency response curves in terms of the modulation amplitudes $\left(b_i\right)$ and detuning parameters $\left(\sigma_i\right)$ for the steady-state condition $\left(\partial b_i/\partial t,\partial\pi_i/\partial t=0\right)$ of Eqs. (5.44)-(5.46) can be obtained by eliminating the phase terms $\left(\pi_i\right)$. The stability of the steady-state solutions can be investigated by following the procedure explained in previous subsection.

5.2.6 RESULTS AND DISCUSSIONS

a) *Modal analysis: eigenfrequencies and eigenspectrums*

The robotic manipulators are involved in variety of operations in diverse environments involving various forcing conditions. Hence, it is of utmost importance to have a better understanding of the behavior of modal parameters of the robotic manipulators such as eigenfrequencies and mode shapes, so that the designer could manipulate the system to work under safe conditions. In circumstances, when the system is subjected to a forcing frequency equal or nearly equal to one of the system natural frequencies, the system tends to vibrate at inadmissible amplitudes which are catastrophic for the system as well as for the operator involved. The manipulation of the system can be accomplished by varying the system parameters and their affect can be visualized by alternating the nondimensional system parameters. The analysis of system dynamics can be better interpreted by having the prior information about the modal parameters which is basic and an essential requirement. The nondimensional eigenfrequencies of the system can be obtained by numerical solution of the transcendental eigenfrequency equation resulting from the condition for the existence of nontrivial solution of equation obtained in subsection 5.2.1. The system parameters can be varied to obtain different configuration of the multi-link manipulators such as changing the material of different links represented by flexural rigidity ratios $\left(\chi_{1,2}\right)$ and beam mass density ratios $\left(\alpha_{M1,2}\right)$, varying the hub-joints stiffness or inertia $\left(\Omega_{h1,2,3}, I_{h1,2,3}\right)$ etc. Manipulators involved in tasks such as lifting or placing of different objects can be viewed as variation of payload parameter at the terminal of the third link $\left(\alpha_{m3}\right)$. The variation of other parameters can be understood in a similar manner. The system eigenfrequencies decreases with the increase in mass of the payload being lifted by manipulator $\left(\alpha_{m3}\right)$, joint inertias $\left(\alpha_{Ih1,2,3}\right)$, beam mass density ratios of the links $\left(\alpha_{M1,2}\right)$ and joint masses $\left(\alpha_{m1,2}\right)$. The increase in flexural rigidity ratios of the links $\left(\chi_{1,2}\right)$ and stiffness of the joint $\left(\Omega_{h1,2,3}\right)$ causes an increase in the values of system eigenfrequencies. Here also, the system eigenfrequencies show a jump at the unit magnitude of the joint frequency which is a condition where the joint dynamics gets decoupled from the link dynamics and the joint tends to behave as a point mass. For higher values of joint frequency, the system tends to vibrate at a higher mode of vibration. The influence of system parameters is significant on the fundamental natural frequencies of the manipulator which may result in the inaccurate predication of resonance phenomenon during the forced interaction of manipulator.

An efficient vibration control and stabilization of a multi-link manipulator (3R) under the influence of various design parameters can be achieved by having a better understanding of variation of vibration spectrums with system parameters. The fundamental characteristics of a mechanism or mechanical structure in modal space are resonant frequencies and the corresponding eigenfunctions. In this section, the unpredictability of the system dynamics under essential parametric variation and subsequent configuration dependency of the system, are inves-

tigated in terms of modal properties. It is obvious that any change in the inertia and stiffness properties of multi-link manipulator leads to variations of the eigenfrequencies and hence directly introduces uncertainty and robustness problems in such manipulators. Hence, the present study shall demonstrate the passive control of the system through the variation of multi-link parameters.

In various industrial applications a robot is utilized to manipulate different payloads and hence the dynamic characteristics of the manipulator depend on the payload. The payload lifted by the manipulator adversely affects the overall inertia of the system which in turn changes the system eigenfrequencies and hence the mode shapes. The influence of payload (α_{m3}) on the 3R manipulator system is illustrated in Fig. 5.2, where the mode shapes of the system are compared with no payload condition. It is clearly evident that the consideration of payload (α_{m3}) significantly affects the all modes of vibrations and the amplitude of the manipulator tip decreases with increase in payload leading to error in the modal displacements of about 30-40 %. The higher modes of vibration remain unaltered with the variation of payload and mode shapes clutter along the length of the manipulator.

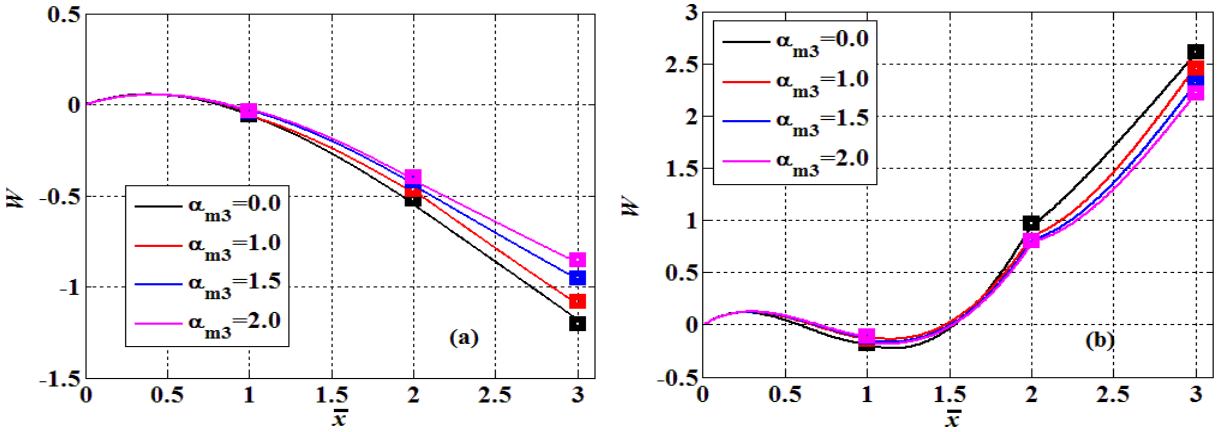

Fig. 5.2: Influence of payload mass parameter (α_{m3}) on mode shapes apes

with $\alpha_{m1,2}=1.0$, $\alpha_{M1,2}=1.0$, $\alpha_{L1,2}=1.0$, $\chi_{1,2}=1.0$, $\Omega_{h1,2,3}=0.5$, , and $\alpha_{Ih1,2,3}=1.0$ (a) mode 1 (b) mode 2.

The variation of mode shapes with the change in beam density of second (α_{M1}) and third link (α_{M2}) is demonstrated in Fig. 5.3. The beam density associated with the links can be maintained by changing the cross sectional area of the link if both the links are of same material. The influence of beam density is prominent in case of higher modes of vibration and mode shapes tend to spread out along the length of manipulator. The amplitude of the higher mode shapes increases with increase in second link beam mass density (α_{M1}), while the amplitude decreases with increase in third link beam mass density parameter (α_{M2}).

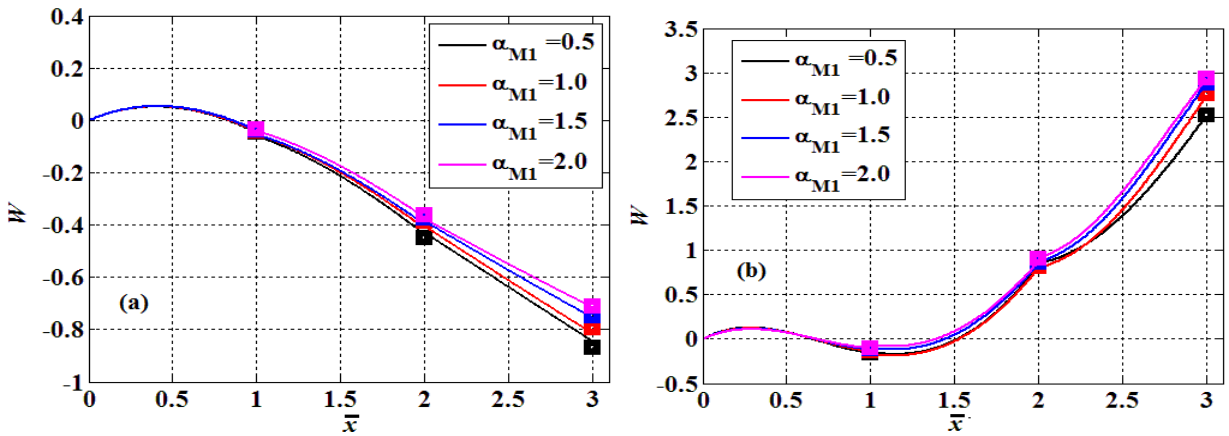

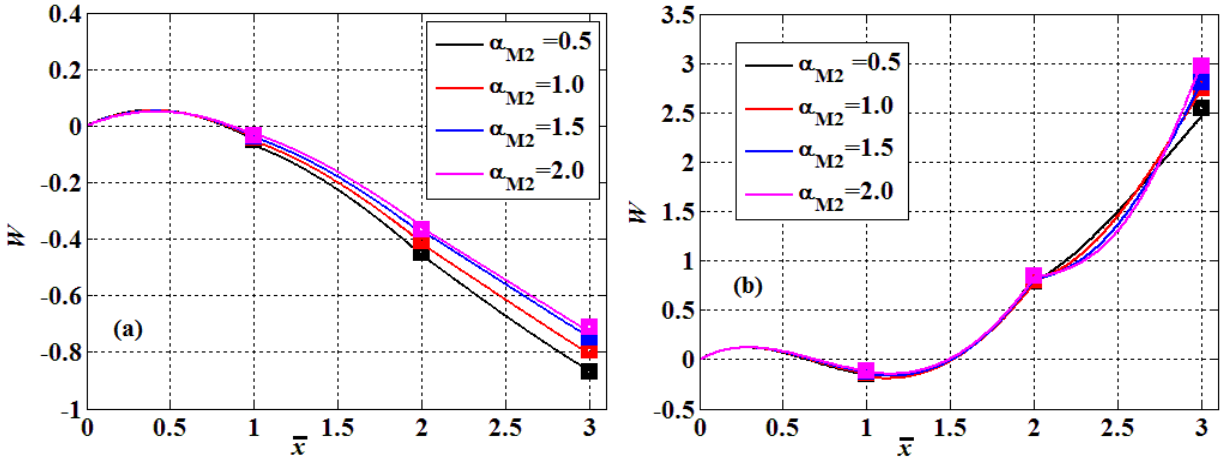

Fig. 5.3: Influence of first and second beam mass density parameter $(\alpha_{M1,2})$ on mode shapes with $\alpha_{m1,2,3}=1.0$, $\chi_{1,2}=1.0$, $\alpha_{L1,2}=1.0$, $\Omega_{h1,2,3}=0.5$, , and $\alpha_{Ih1,2,3}=1.0$ (a) mode 1 (b) mode 2.

The variation of system mode shapes with flexibility of the second link and third link$(\chi_{1,2})$ with respect to the first link is shown in Fig. 5.4. It is evident from the figure that both the flexural rigidity ratio of second link and third link immensely affect the modes of vibration. The amplitude of manipulator decreases with the increase in the second link flexural rigidity ratio(χ_1) and the third link flexural rigidity ratio(χ_2). The higher modes of vibration in second case clutter together nullifying the effect of the change in(χ_2), unlike the case of second link flexural rigidity ratio(χ_1).

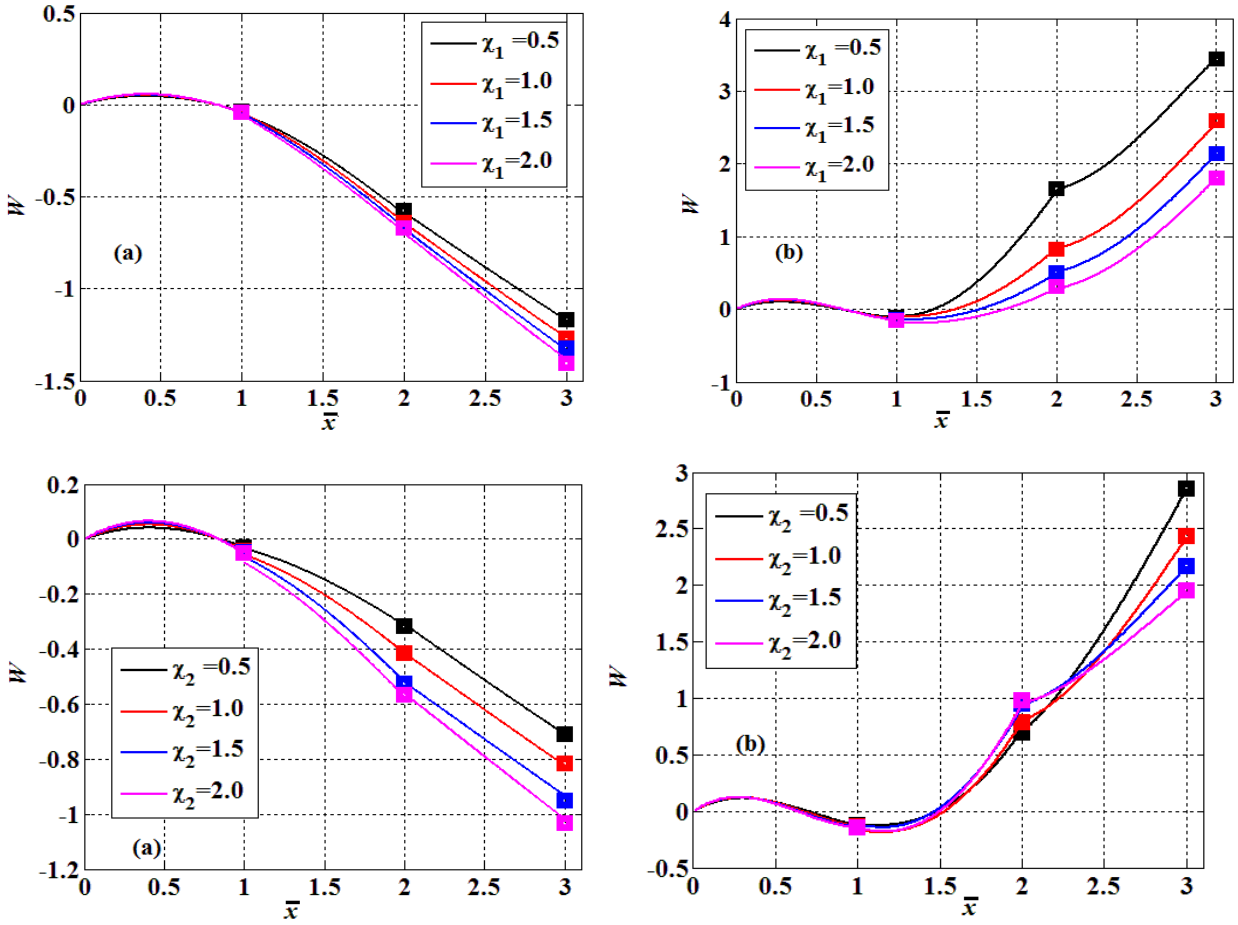

Fig. 5.4: Influence of flexural rigidity ratios $(\chi_{1,2})$ on mode shapes with $\alpha_{m1,2,3}=1.0$, $\alpha_{M1,2}=1.0$, $\alpha_{L1,2}=1.0$, $\Omega_{h1,2,3}=0.5$, and $\alpha_{Ih1,2,3}=1.0$ (a) mode 1 (b) mode 2.

In Fig. 5.5, the influence of hub inertia $(\alpha_{Ih2,3})$ on the mode shapes of the system is demonstrated. It is evident; that the hub inertia affects the lower modes of vibration significantly while the amplitude of the system decreases with the increase in hub inertia This effect is noticeable only for the larger range of lower eigenfrequencies. The variation of hub-joint frequency $(\Omega_{h1,3})$ of system can be regarded as the variation of joint stiffness. Unit magnitude of joint parameters is the limiting case when Eqs. (5.17)-(5.19) becomes invalid and hub-joint dynamics gets decoupled from the manipulator dynamics which in turn compels the joints and hub to behave like concentrated masses. The eigenfunctions for this limiting case have to be calculated by considering the manipulator having point masses at the joints and neglecting the revolute motion of the joints. It has already been noticed that the system changes its behavior for the frequency parameter values between 1 and 1.5. The influence of system eigenspectrum with hub (Ω_{h1}) and second joint frequency $(\Omega_{h3})$is shown in Fig. 5.6. The change in hub frequency (Ω_{h1}) is indicative of a significant effect on the deflection of manipulator and the amplitude of the proximal end of the manipulator increases with increase in(Ω_{h1}). A change in behavior of the manipulator is visible at Ω_{h3} =1.5 due to a sudden jump in eigenfrequencies as discussed in previous section. For second joint frequency parameter values of 1.0< Ω_{h3} <1.5, the system vibrates at higher mode of vibration for the corresponding eigenfrequency.

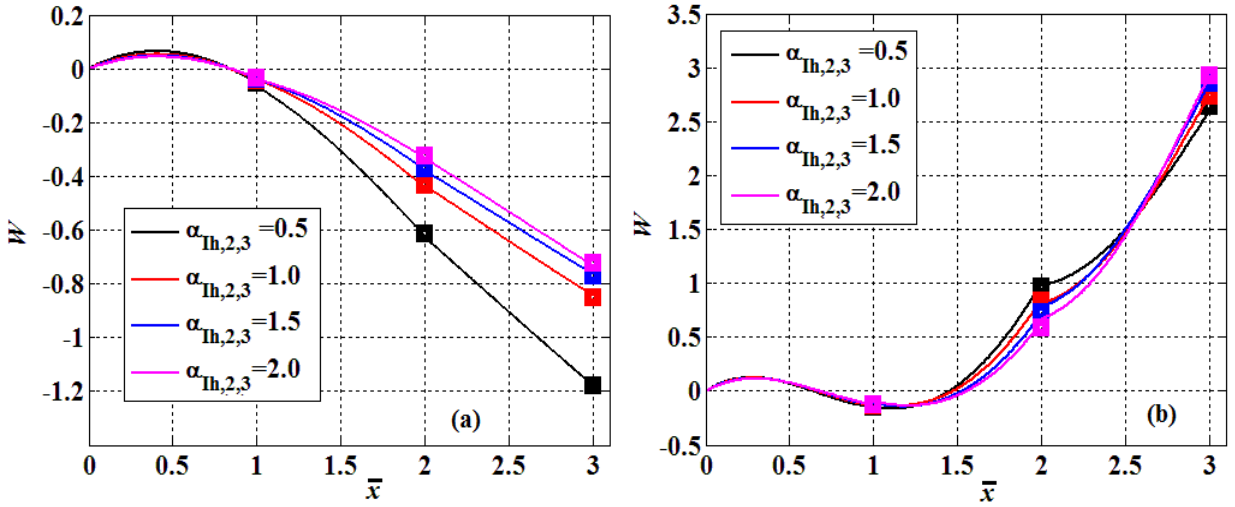

Fig. 5.5: Influence of hub joint inertia parameters $(\alpha_{Ih2,3})$ on mode shapes with $\alpha_{m1,2,3}=1.0$, $\alpha_{M1,2}=1.0$, $\alpha_{L1,2}=1.0$, $\chi_{1,2}=1.0$, and $\Omega_{h1,2,3}=1.0$ (a) mode 1 (b) mode 2.

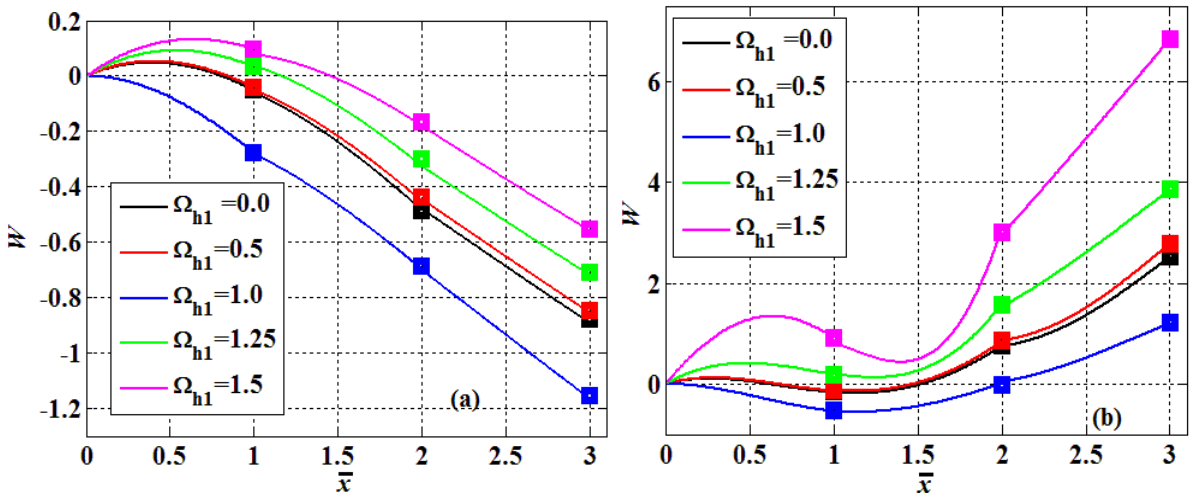

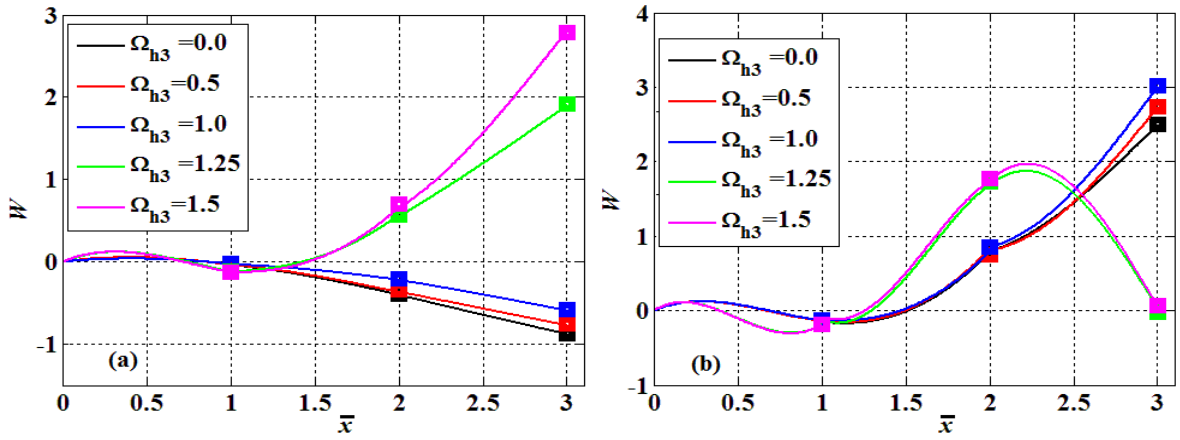

Fig. 5.6: Influence of hub joint frequency parameter $(\Omega_{1,3})$ on mode shapes with $\alpha_{m1,2,3}=1.0$, $\alpha_{M1,2}=1.0$, $\alpha_{L1,2}=1.0$, $\alpha_{Ih1,2,3}=1.0$, $\chi_{1,2}=1.0$, and $\Omega_{h2}=1.0$ (a) mode 1 (b) mode 2.

The determination of eigencharacteristics plays a significant role in many applications such as design, control and identifications of flexible manipulators. The first eigenfrequency is most important vibration mode regarding control of flexible manipulators as it imposes the limitation on the system to maneuver at higher speeds. Also, control algorithm such as command shaping depends on the accurate determination of first eigenfrequency and the corresponding eigenfunctions. Hence, the manipulator system can be modified to enhance its performance by manipulating the eigenfrequencies. Also, the evaluation of eigenfrequencies and corresponding mode shapes enables the design engineer to have a provision for the adjustment in the system by varying system parameters when forcing frequency becomes equal or nearly equal to one of the natural frequencies of the manipulator resulting in the phenomenon called resonance.

b) *System performance: tip Responses*

Here, the closed form of equations obtained as Eq. (5.23) is numerically simulated to analyze the system responses, i.e., angular tip positions, tip displacements and angular accelerations of the links, under externally applied joint torques for better understanding of the system dynamics while achieving the desired set points. The system responses are significantly affected by the change in the manipulator configurations and parameters which in turn influence the effectiveness of the manipulator performance. Smooth sinusoidal torque of amplitude 0.1 N-m, 0.2 N-m, and 0.3 N-m with a duty cycle of 2 seconds is applied at the first, second and third hub joint, respectively. The geometric and physical characteristics of the manipulator considered for the simulations are density of the links $(\rho_{1,2,3})$ as 7800 kg/m^3, length of the links as $(L_{1,2,3})$ 0.5m, Young's modulus of material of links as $(E_{1,2,3})$ 240 GPa, mass moment of inertia of links as $(I_{h1,2,3})$ 0.008 kg/m^2, and masses at the terminal of the links $(m_{1,2,3})$ as 0.1 kg. The parametric variations of the time responses are depicted in Fig. 5.7-Fig. 5.10 for different system parameters. From Fig. 5.7 it can be observed that the angular tip position of the links and the settling time decreases with increase in payload mass. The increase in payload mass increases the total inertia of the system and hence the amplitude of the tip acceleration decreases. However, vibrations in the tip after the duty cycle of the torque in case of the terminal link are observed to be larger as compared to the first link. Hence, it can also be concluded that, as the number of links are increased in the manipulator, end tip vibrations increase and therefore more effective control techniques have to be adopted for the last link as compared to the first link. Due to its involved dynamics in the first and second link boundary conditions, the third joint mass only affects the first and second links which is noticeable in Fig. 5.8. The angular positions and the settling time of the first and second link decrease with the third joint mass leading to significant position inaccuracy of the manipulator.

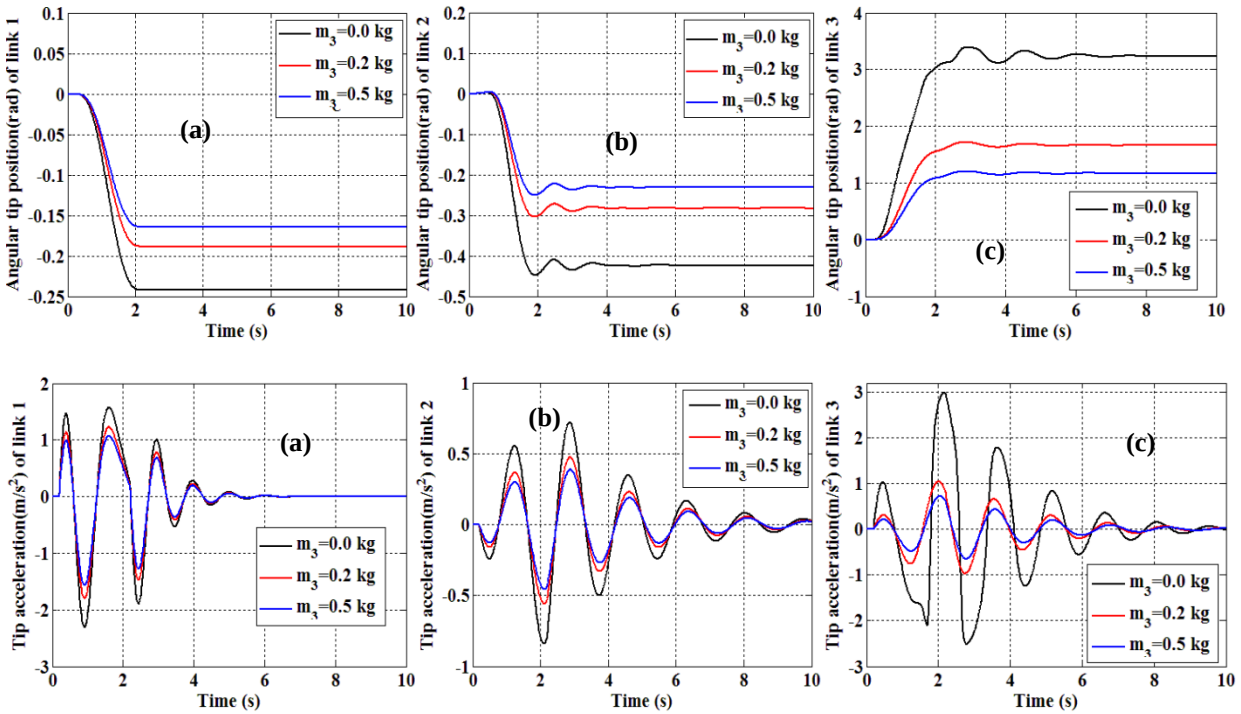

Fig. 5.7: Influence of payload mass (m_3) on the angular positions and tip accelerations of the (a) first link (b) second link (c) third linkthe links.

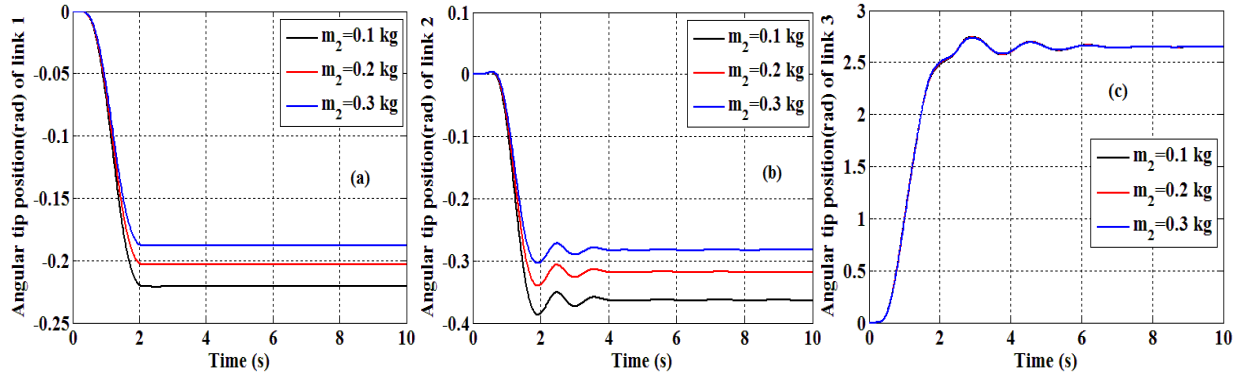

Fig. 5.8: Influence third joint mass (m_2) on the angular positions of the (a) first link (b) second link (c) third link.the links.

The variation of system response with the change in joint inertia is shown in Fig. 5.9. It is observed that the angular tip position decreases with the increase in joint inertias. As the number of links of the manipulator is increased, the effect of change in joint inertia on the end point accelarations increases. The tip of the third link experience large residual vibrations as compared to the first link after the duty cycle of the respective torques.

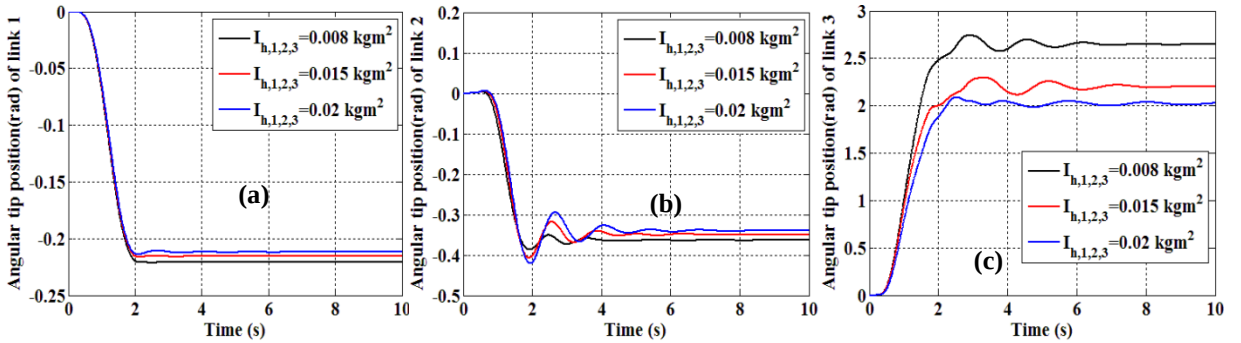

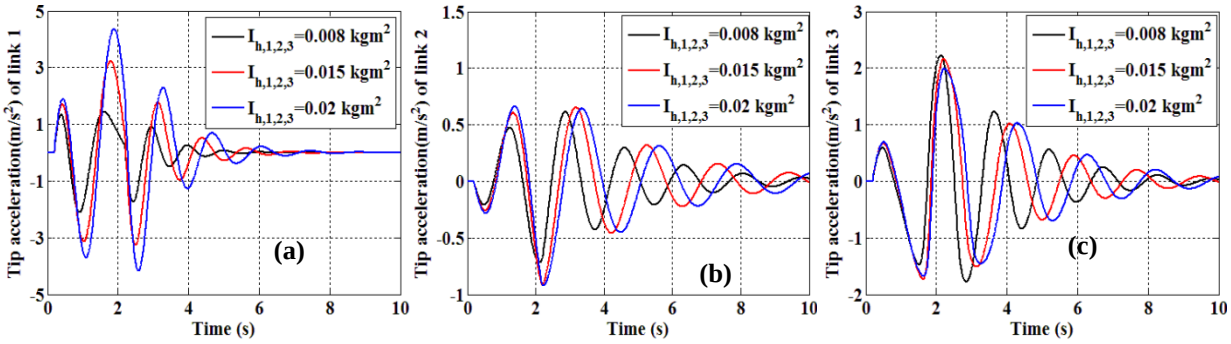

Fig. 5.9: Influence joint inertias $\left(I_{h1,2,3}\right)$ on the angular positions and tip accelerations of the (a) first link (b) second link (c) third link.the links.

The variation in length of the manipulator links has a significant influence on the angular position of the respective link which is also evident in Fig. 5.10. The increase in length of the second link decreases the angular tip position of the links and this effect is most prominent in the case of second link tip response. In the case of first link, the residual vibration damp out after 5 seconds, but in the case of second and third links the rigid vibrations of the tip increases which may cause the inaccuracies in the tip positioning. The study of the tip responses due to the input torque shall contribute to the enhancement of effective control techniques for PRR and long reach manipulators. It is also observed that as the increase in the length of the manipulator induces inaccuracies in the tip position due to parametric variations, the control engineer has to appropriately design the controllers to suppress or attenuate the residual vibrations in the manipulators, especially for use in precision industries.

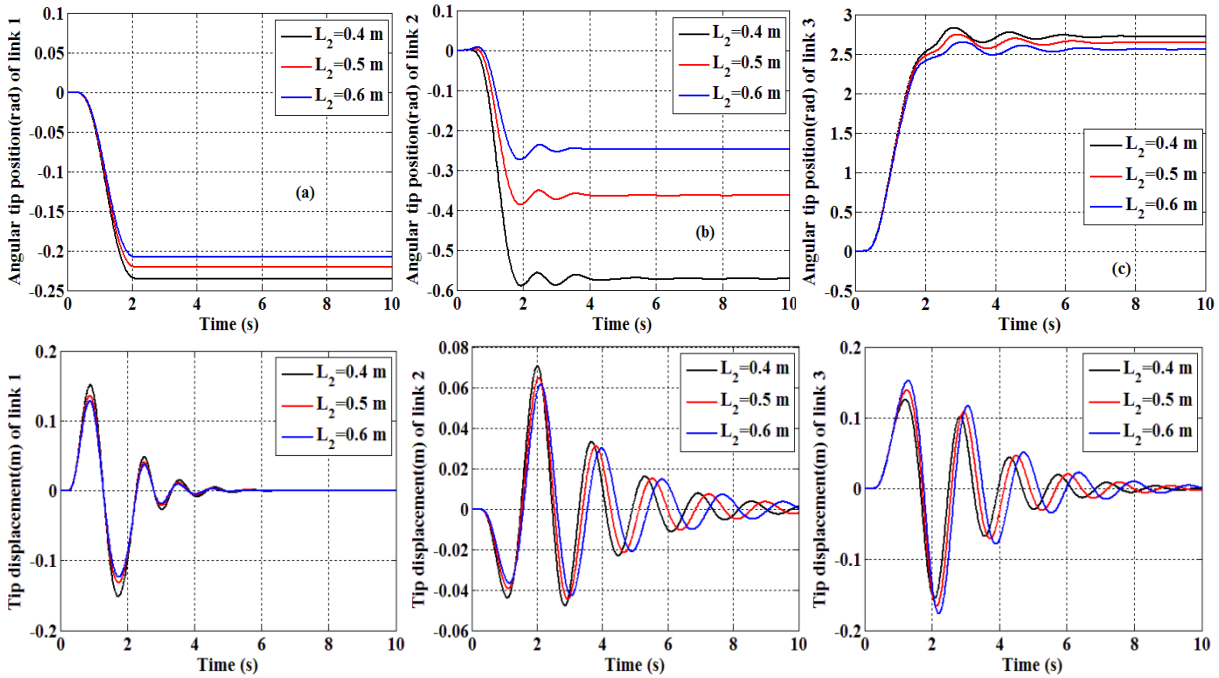

Fig. 5.10: Influence length of links $\left(L_2\right)$ on the angular positions and modal displacements of the links. the (a) first link (b) second link (c) third link.

c) *Nonlinear analysis: bifurcation and stability*

The geometrical and physical properties of the links considered for the simulations and frequency response curves are similar to the subsection 4.4.5. The nondimensional damping coefficients $\left(\xi_{1,2}\right)$, amplitude of the revolute motion of joints $\theta_{10,20,30}$, small book keeping parame-

ter (ε) and scaling factor (r) are chosen as 0.01, 0.0005, 0.1 and 0.005, respectively. The other parameters have been indicated in the figures or captions. To avoid the internal resonance the length parameters for the second (α_{L1}) and third link (α_{L2}) is taken as 1.1 and 1.2, respectively. The bifurcation diagrams for the internal resonance arising due to the inertial coupling between the links and the primary resonance due to the revolute motion of the joints are illustrated in Fig. 5.11-Fig. 5.24. The representative frequency response curves for the internal resonance in second link and primary resonance in first link have been shown in Fig. 5.11.

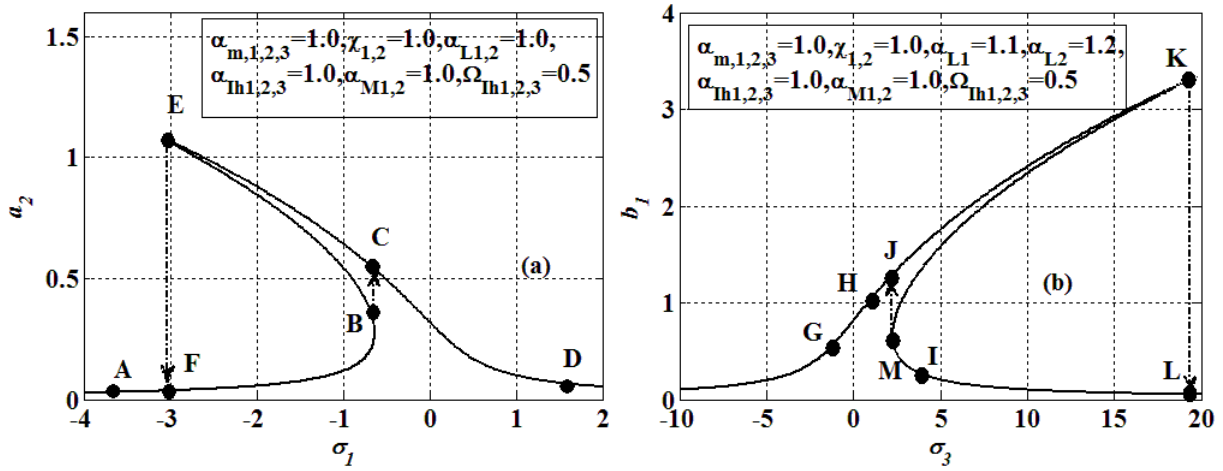

Fig. 5.11: Frequency response curves of (a) the second and first link for internal resonance and (b) the first link for primary resonance, respectively.

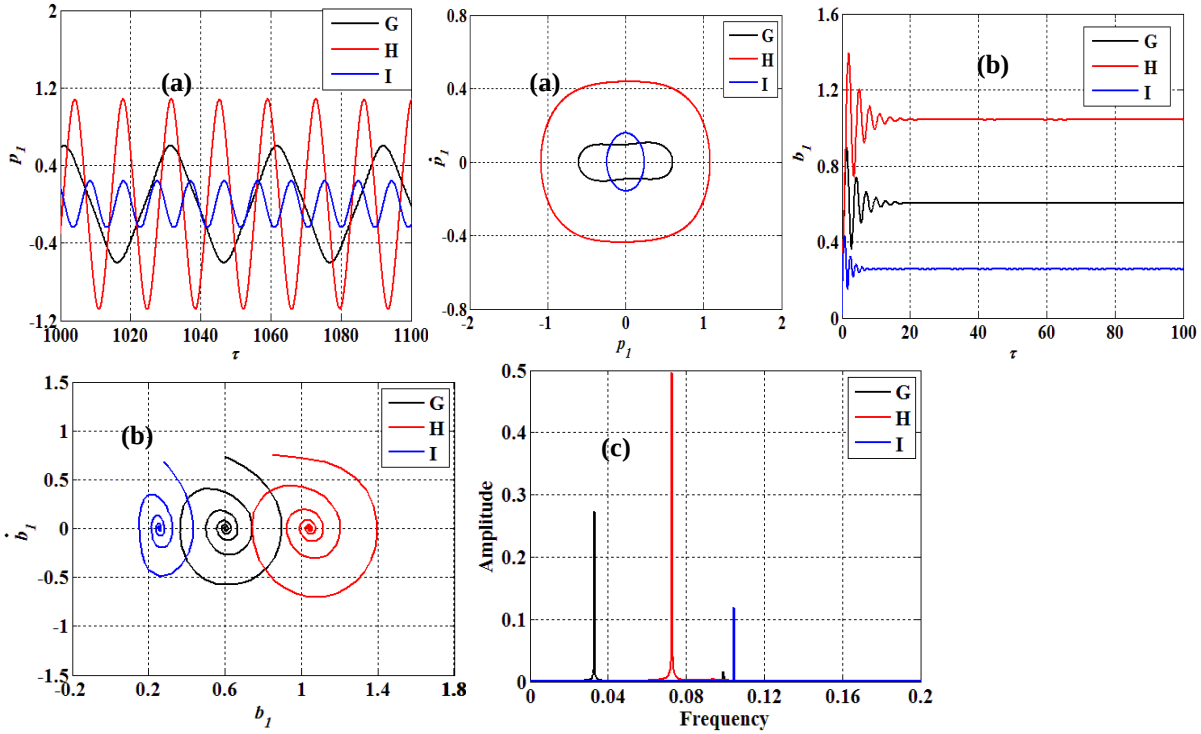

Fig. 5.[SEQ Fig. * ARABIC \s 1 [12[: (a) Numerical and (b) analytical time histories, phase portrait and (c) FFT of critical points G, H, and I identified inkeyed to Fig. 5.11.

In all figures the dashed line represents the unstable solutions while solid line depicts stable solutions. The system exhibits multi-valued solutions and jump phenomenon due to saddle-node bifurcations for the existence of geometrical nonlinearities. Spring softening and spring-hardening behaviors are observed in second and first link for internal and primary resonance case, respectively. The jump up and jump down phenomena occurring while the starting or stopping of the prime mover may result in the catastrophic failure of the manipulator system. The time response, phase portrait and FFT's obtained by numerically solving Eq. (5.24)

have been compared in Fig. 5.12 with the corresponding analytical results determined from reduced equations of the amplitude and phase accomplished in Eq. (5.44) at the various critical points (G, H, I) as identified in Fig. 5.11 and found to be in good agreement. Further, the influence of system characteristics on the frequency response curves of the links for internal resonance and primary resonance case has been examined in order to have a better understanding of ways to attenuate unwanted vibrations by operating the system in safe zones.

Now, firstly, the influence of system parameters on the nonlinear behavior of the system through frequency response curves for the internal resonance case and in later part the primary resonance is studied. The effect of the initial excitations (a_1) given to the first link on the frequency response of the second and third links is depicted in Fig. 5.13. The amplitude of both the links at a particular frequency and the unstable regions increase with increase in the amplitude of the excitations. As the mass of the payload (α_{m3}) lifted by the manipulator increases, the jump length decreases for both links leading to smaller unstable region and the links tend to vibrate at lower amplitudes at a particular frequency which is also noticeable in Fig. 5.14. The comparison has been made with respect to the no payload condition $(\alpha_{m3}=0)$ and the jump phenomenon occurs at much lower frequency as the payload mass (α_{m3}) is increased.

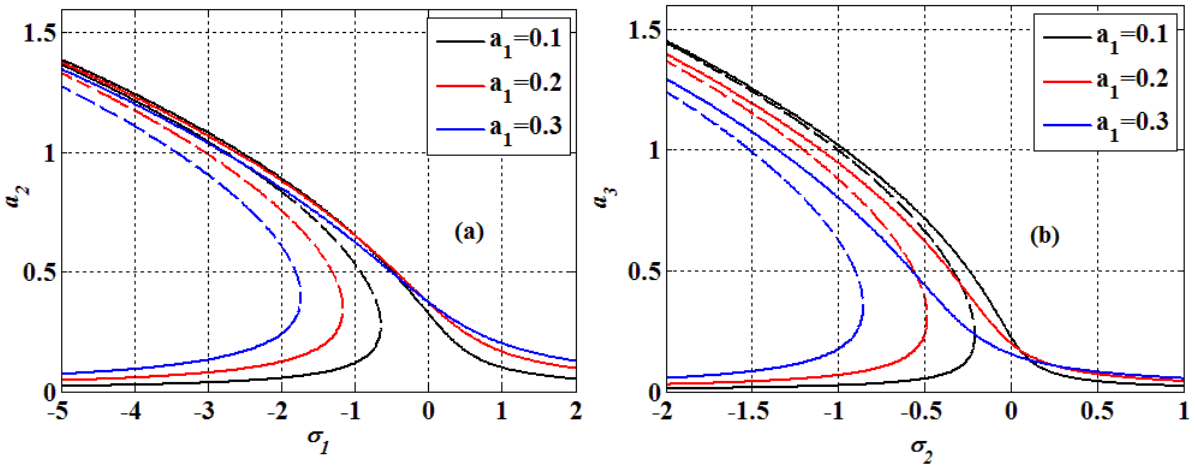

Fig. 5.13: Influence of initial excitation (a_1) on frequency response curves of (a) second and (b) third link for internal resonance with $\alpha_{m1,2,3}=1.0$, $\alpha_{M1,2}=1.0$, $\chi_{1,2}=1.0$, $\alpha_{L1,2}=1.0$, $\Omega_{h1,2,3}=0.5$, and $\alpha_{Ih1,2,3}=1.0$.

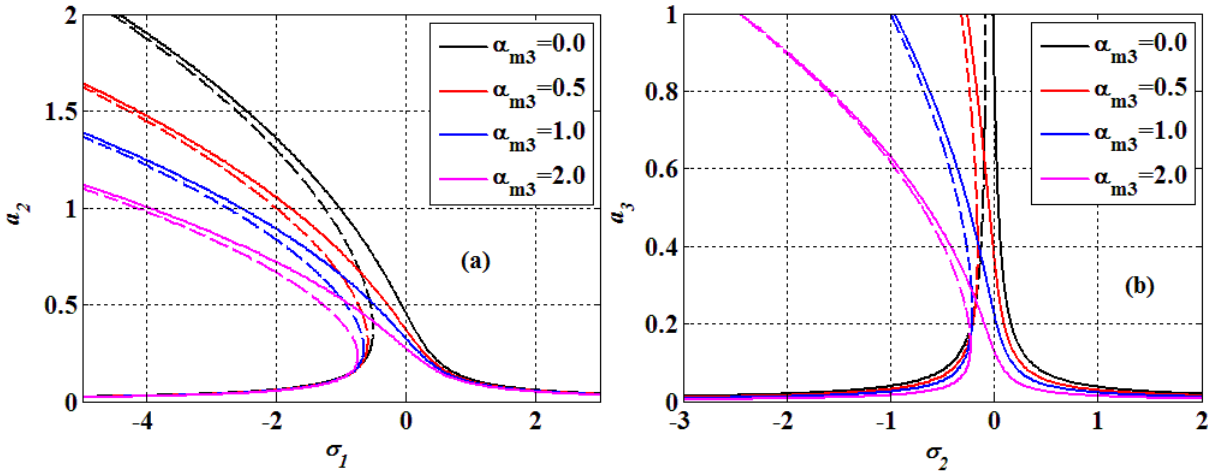

Fig. 5.14: Influence of payload mass (α_{m3}) on frequency response curves of (a) second and (b) third link for internal resonance with $\alpha_{m1,2}=1.0$, $\alpha_{M1,2}=1.0$, $\chi_{1,2}=1.0$, $\alpha_{L1,2}=1.0$, $\Omega_{h1,2,3}=0.5$, and $\alpha_{Ih1,2,3}=1.0$.

The flexural rigidity $(\chi_{1,2})$ and beam mass density $(\alpha_{M1,2})$ ratio of the links can be varied by changing the cross-sectional dimensions of the links. The influence of variation in flexur-

al rigidity (χ_1) on the frequency response curves is illustrated in Fig. 5.15. It is observed that, while the amplitude of the first link at a particular frequency increases, the amplitude of the second link decreases with the increase in flexural rigidity (χ_1). A negligible effect of flexural rigidity ratio (χ_2) on the frequency response of the second link is noticed, but the jump length in case of link increases with the increase in flexural rigidity ratio of the third link. It can be observed from Fig. 5.16 that the beam mass density of the third link (α_{M2}) significantly affects the frequency response of both links, and the steady-state amplitude of the second link at a specific frequency increases while that of the third link decreases.

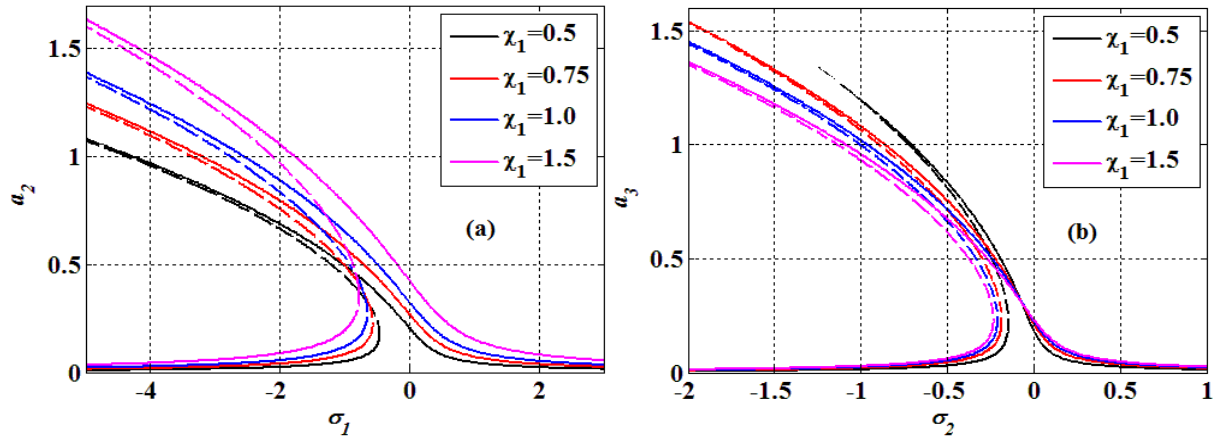

Fig. 5.15: Influence of second link flexural rigidity ratio (χ_1) on frequency response curves of (a) second and (b) third link for internal resonance with $\alpha_{m1,2,3}=1.0$, $\alpha_{M1,2}=1.0$, $\chi_2=1.0$, $\alpha_{L1,2}=1.0$, $\Omega_{h1,2,3}=0.5$, and $\alpha_{Ih1,2,3}=1.0$.

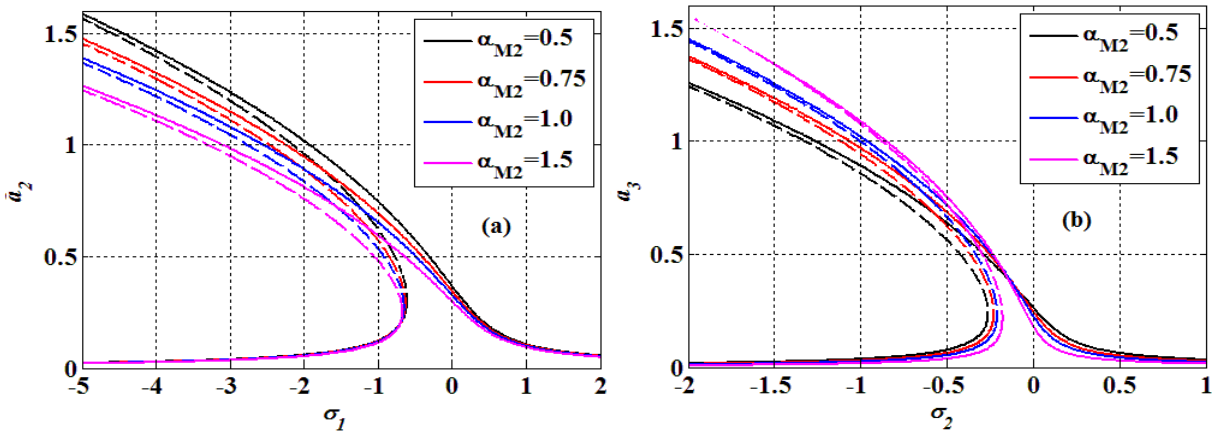

Fig. 5.16: Influence of third link beam mass density parameter (α_{M2}) on frequency response curves of (a) second and (b) third link for internal resonance with $\alpha_{m1,2,3}=1.0$, $\alpha_{M1}=1.0$, $\chi_{1,2}=1.0$, $\alpha_{L1,2}=1.0$, $\Omega_{h1,2,3}=0.5$, and $\alpha_{Ih1,2,3}=1.0$.

The jump length of both links increase with increase in joint inertias $(\alpha_{Ih1,2,3})$ which is also demonstrated in Fig. 5.17. For the third link the unstable region is very small and the system vibrates at very small amplitude for small values of joint inertias $(\alpha_{Ih1,2,3})$. The first joint frequency (Ω_{Ih1}) has a negligible influence on the steady-state response of the second link which is also depicted in Fig. 5.18. In the case of third link, the amplitude at a specific frequency first increases up to the unit magnitude of Ω_{h1} $(\Omega_{h1}=1)$ and with the further increase in Ω_{h1} results in decrease in the jump length. It can be observed that no behavior changes occur in the second and third link for the internal resonance case and both the manipulator exhibit spring softening behavior for parametric variations.

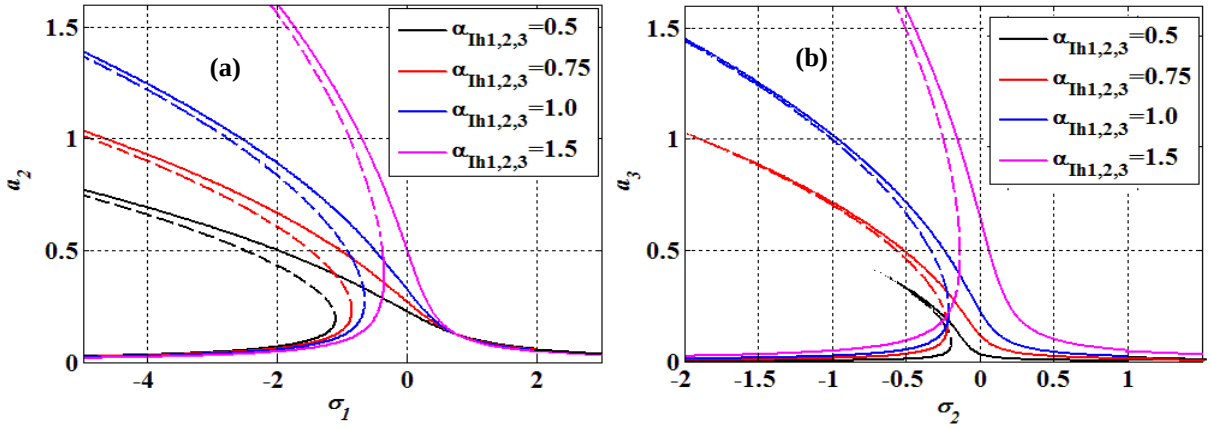

Fig. 5.17: Influence of hub and joint inertia parameter $(\alpha_{Ih1,2,3})$ on frequency response curves of (a) second and (b) third link for internal resonance with $\alpha_{m1,2,3}=1.0$, $\alpha_{M1,2}=1.0$, $\chi_{1,2}=1.0$, $\alpha_{L1,2}=1.0$, and $\Omega_{h1,2,3}=0.5$.

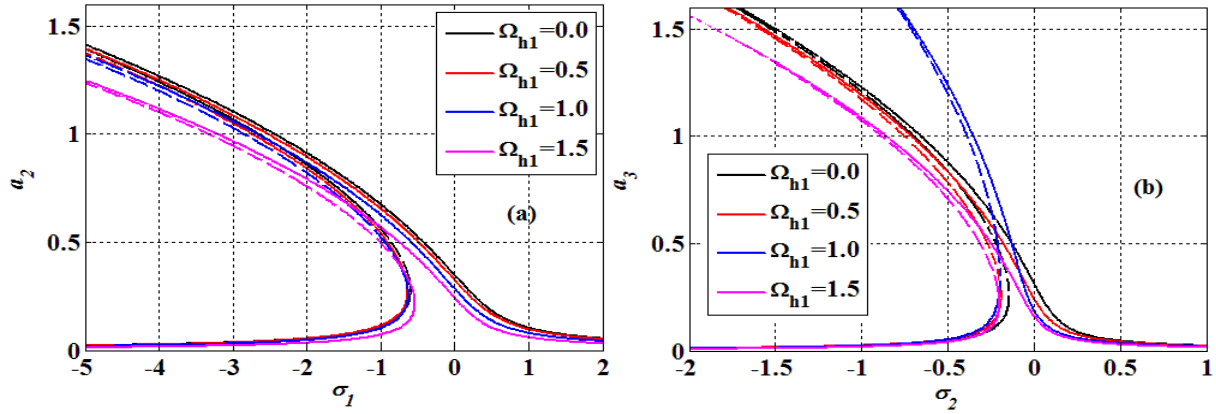

Fig. 5.18: Influence of first hub joint frequency parameter (Ω_{h1}) on frequency response curves of (a) second and (b) third link for internal resonance with $\alpha_{m1,2,3}=1.0$, $\alpha_{M1,2}=1.0$, $\chi_{1,2}=1.0$, $\alpha_{L1,2}=1.0$, $\Omega_{h2,3}=0.5$. and $\alpha_{Ih1,2,3}=1.0$.

The first link experiences behavior alteration as shown in Fig. 5.19; from spring softening to spring hardening with increase in payload (α_{m3}) for the primary resonance in the link arising due to the revolute motions given to the joints. For no payload condition $(\alpha_{m3}=0)$, the jump length and the unstable region is much smaller in the case of the second and third links. It is noticed that the first link demonstrate spring softening behavior while the second and third links show spring hardening behavior for the variation of second link flexural rigidity ratio (χ_1) as illustrated in Fig. 5.20. While a marginal change is noticed in the amplitude of the first link, the amplitude of the second and third links respectively increase and decrease with increase in flexural rigidity ratio (χ_1).

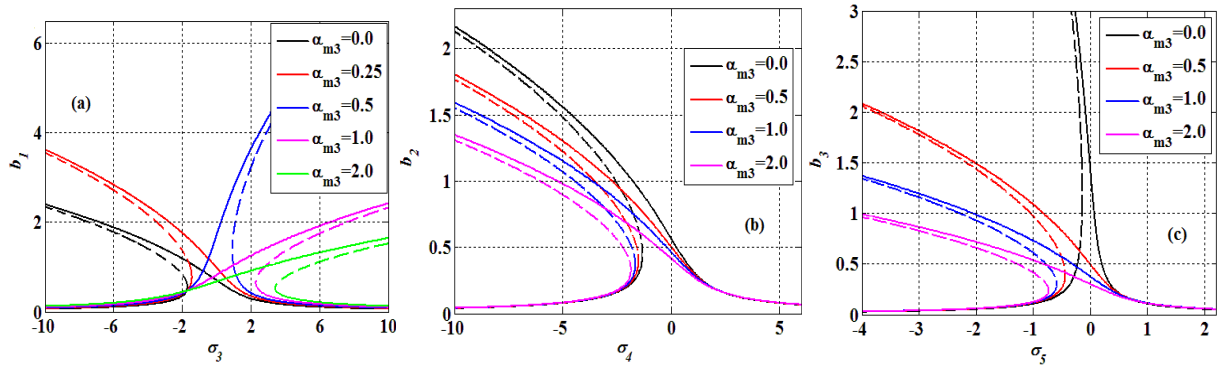

Fig. 5.19: Influence of payload mass (α_{m3}) on frequency response curves of (a) first, (b) second and (c) third link for simple resonance with $\alpha_{m1,2}=1.0,\ \alpha_{M1,2}=1.0,\ \chi_{1,2}=1.0,\ \alpha_{L1}=1.1,\ \alpha_{L2}=1.2,\ \Omega_{h1,2,3}=0.5,$ and $\alpha_{Ih1,2,3}=1.0.$

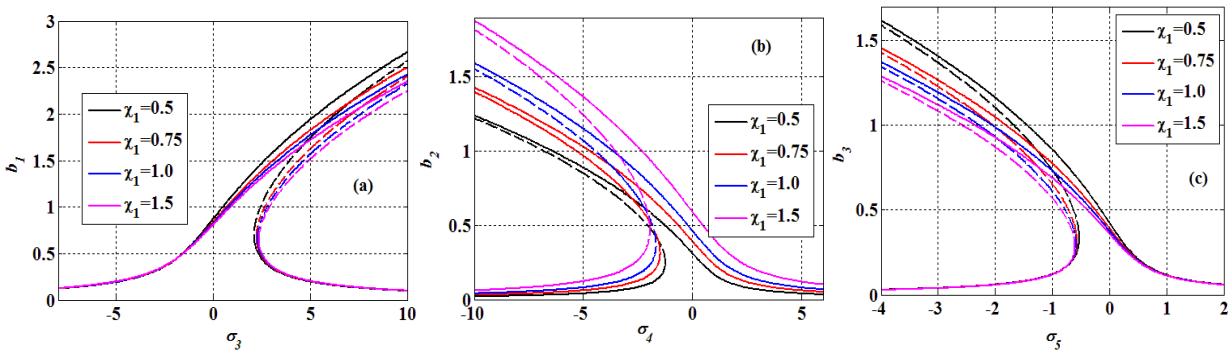

Fig. 5.20: Influence of second link flexural rigidity ratio (χ_1) on frequency response curves of (a) first, (b) second and (c) third link for simple resonance with $\alpha_{m1,2,3}=1.0,\ \alpha_{M1,2}=1.0,\ \chi_2=1.0,\ \alpha_{L1}=1.1,\ \alpha_{L2}=1.2,\ \Omega_{h1,2,3}=0.5,$ $\alpha_{Ih1,2,3}=1.0.$

The first link changes its behavior from spring softening to spring hardening and the amplitude of the second link at a particular frequency increases with the increase in beam mass density of the second link (α_{M1}) which is evident from Fig. 5.21. This behavior alteration can lead to significant increase or decrease in manipulator vibrations while under operating conditions and may damage the system if appropriate trend is not maintained. Also, as the beam mass density (α_{M1}) is increased, the frequency range at which the jump phenomenon occurs also increases. A negligible effect on the frequency response of the third link is seen with the change of beam mass density (α_{M1}). Mostly, it is noticed that the nonlinear behavior of the first link is affected by the various system parameters. In the case of lower values of joint inertia parameters, the system exhibits spring hardening behavior and for higher values of $\alpha_{Ih1,2,3}$ the system changes its behavior to spring softening as shown in Fig. 5.22. The amplitudes of other the two links increases with the increase in $\alpha_{Ih1,2,3}$ at a particular detuning parameter.

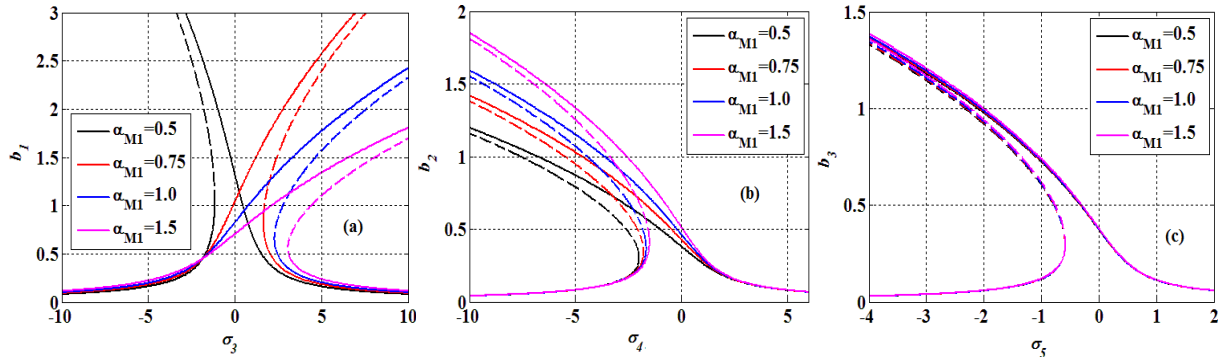

Fig. 5.21: Influence of second link beam mass density parameter (α_{M1}) on frequency response curves of (a) first, (b) second and (c) third link for simple resonance with $\alpha_{m1,2,3}=1.0,\ \alpha_{M2}=1.0,\ \chi_{1,2}=1.0,\ \alpha_{L1}=1.1,\ \alpha_{L2}=1.2,\ \Omega_{h1,2,3}=0.5,$ and $\alpha_{Ih1,2,3}=1.0.$

The variation of frequency response of the links of a 3R manipulator with the first and third joint frequencies $(\Omega_{h1,3})$ is shown in Fig. 5.23-Fig. 5.24. The increase in first joint frequency parameter (Ω_{h1}) causes a change in the behavior of the first link from spring softening to spring hardening with a marginal influence on the jump length of the second and third links. It is also observed that the S-N bifurcation point for the second and third link almost occurs at the same point. The third joint frequency (Ω_{h3}) alters the behavior from spring softening to spring

hardening for second and third links. However, in the case of the first link, the behavior change is seen only around the unit magnitude (Ω_{h3} =1.0), of the third joint frequency parameter.

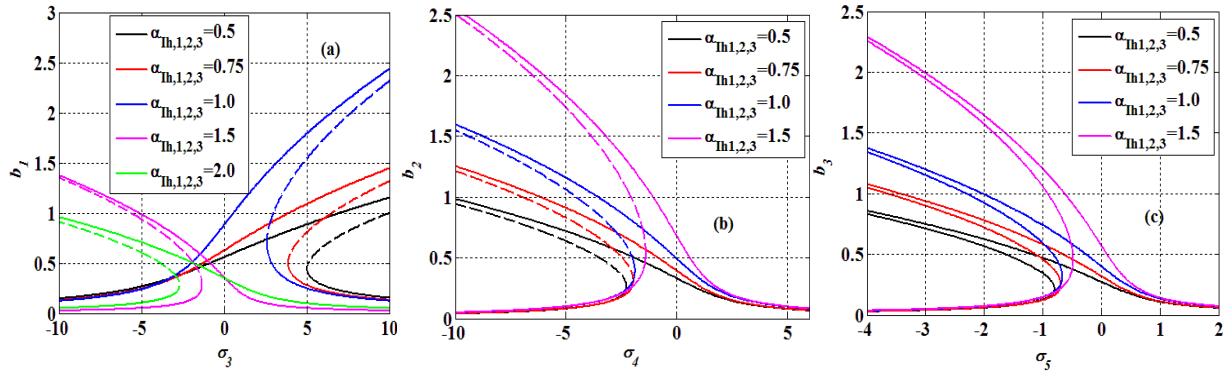

Fig. 5.22: Influence of hub and joint inertia parameter $(\alpha_{Ih1,2,3})$ on frequency response curves of (a) first, (b) second and (c) third link for simple resonance with $\alpha_{m1,2,3}=1.0$, $\alpha_{M1,2}=1.0$, $\chi_{1,2}=1.0$, $\alpha_{L1}=1.1$, $\alpha_{L2}=1.2$, and $\Omega_{h1,2,3}=0.5$.

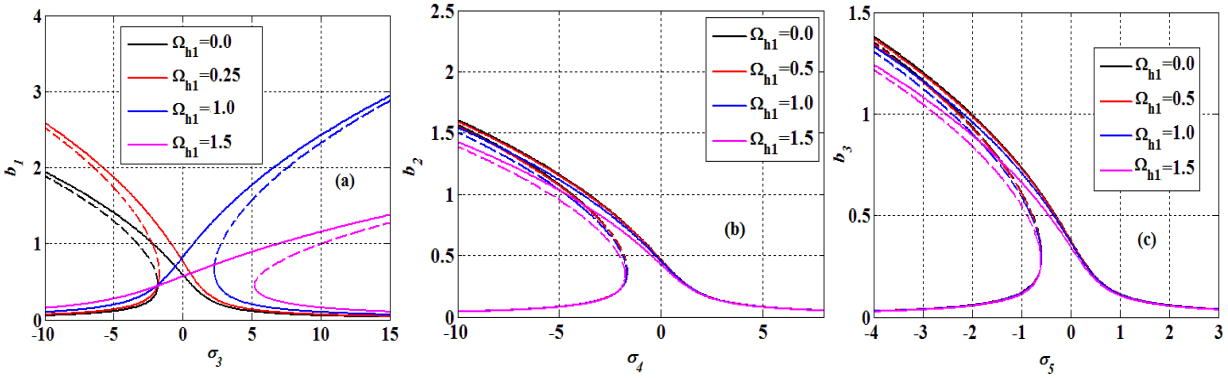

Fig. 5.23 : Influence of first hub joint frequency parameter (Ω_{h1}) on frequency response curves of (a) first, (b) second and (c) third link for simple resonance with $\alpha_{m1,2,3}=1.0$, $\alpha_{M1,2}=1.0$, $\chi_{1,2}=1.0$, $\alpha_{L1}=1.1$, $\alpha_{L2}=1.2$, $\Omega_{h2,3}=0.5$ and $\alpha_{Ih1,2,3}=1.0$.

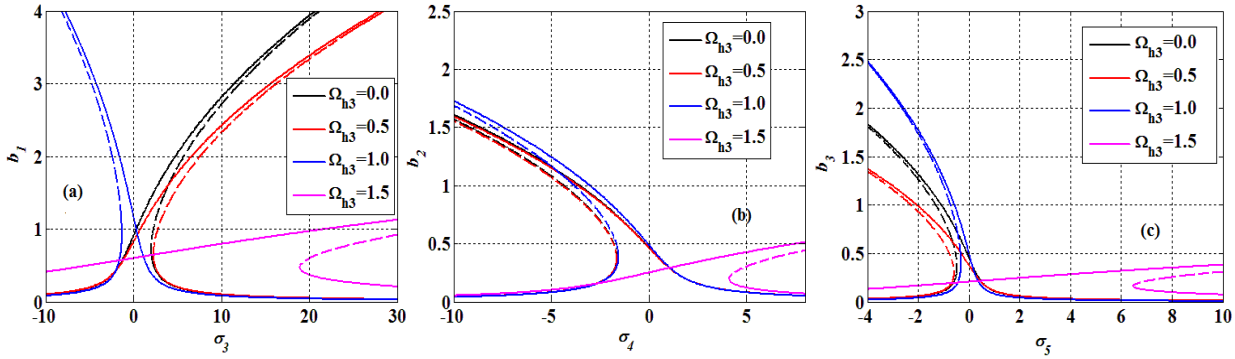

Fig. 5.24: Influence of third hub joint frequency parameter (Ω_{h3}) on frequency response curves of (a) first, (b) second and (c) third link for simple resonance with $\alpha_{m1,2,3}=1.0$, $\alpha_{M1,2}=1.0$, $\chi_{1,2}=1.0$, $\alpha_{L1}=1.1$, $\alpha_{L2}=1.2$, $\Omega_{h1,2}=0.5$ and $\alpha_{Ih1,2,3}=1.0$.

5.3 SUMMARY

This work presents a theoretical framework to dynamically model a multi-link flexible manipulator having harmonic prismatic and revolute joints and undergoing a bidirectional time dependent motion. The influence of system parameters on the modal characteristics of 3R manipulator are examined.

The eigenfrequencies decrease with the increase in inertia of the system due to addition of payload mass, joint inertia and beam mass density of the second and third links. The eigenfrequencies increase with increase in system stiffness as the flexural rigidity ratio associated with the links and stiffness of the joints is increased. A sudden jump in the eigenfrequencies is observed at the unit magnitude of joint frequency parameter. The deflection of the manipulator is significantly affected by the change in the mass of payload and system mass parameters. The influence of the payload on the higher modes of vibration is observed to be negligible and cluttering of the mode shapes is noticed. The change in beam mass density and flexural rigidity of the links majorly affects the higher modes of vibration and the amplitude of the manipulator decreases with the increase in joint inertia. At certain values of joint frequency parameter the system changes it behavior adversely and starts vibrating at higher modes of vibration to the corresponding eigenfrequency. The decoupling of joint dynamics from the system is observed for the unit magnitude of the joint frequency parameters and the joints start acting like concentrated mass.

The system responses such as angular tip positions, modal displacements and tip accelerations under parametric variations for the input torque are reported to comprehend the dynamic behavior of the system while reaching the desired positions. The links achieve a lower angular position for the increased payload mass, joint inertias, and link lengths when same amount of torque is applied to the joints. The amplitude of the link tip accelerations increase with the increase in number of links in the manipulator which may cause the increased interaction forces with the working surface. The higher residual vibrations are noticed for the longer link lengths leading to the inaccurate positioning of the long reach manipulators.

The influence of system parameters on the nonlinear behavior and bifurcations of the 3R manipulator for internal resonance incurring due to inertial coupling between the links and primary resonance as a result of harmonic motion of the joints have been studied. The second and third links demonstrate spring softening behavior, leading to multiple solutions and jump phenomena on account of geometric nonlinearities in the links for the internal resonance. While the amplitude and the unstable region of the second link increase with the initial excitations given to the first link, flexural rigidity ratio of second link, and joint inertia parameters, the jump length of the third link increase with the increase in beam mass density ratio of the third link and joint inertias. Unlike the internal resonance case where both links exhibit spring softening behavior with parametric variations, the frequency response curves of first link reveals the behavior alteration from spring softening to spring hardening or vice-versa with the change in payload mass, beam mass density ratio, joint inertias and joint parameters in case of primary resonance.